Synthesis of Rectangular Waveguide Filters With Smooth Profile Oriented to Direct Metal Additive Manufacturing

Jon M. Percaz, *Member, IEEE*, Jabir Hussain, Ivan Arregui, *Member, IEEE*, Fernando Teberio, *Member, IEEE*, David Benito, Petronilo Martin-Iglesias, *Senior Member, IEEE*, Israel Arnedo, *Senior Member, IEEE*, Miguel A. G. Laso, *Senior Member, IEEE*, and Txema Lopetegi, *Member, IEEE*

***Abstract*— In this article, a novel design method for rectangular waveguide filters intended for fabrication using direct metal additive manufacturing (AM) is proposed. The synthesized filters will feature a smooth profile that allows us to fabricate them orienting the filter propagation axis in the vertical building direction, achieving an optimum configuration for direct metal AM fabrication. The novel design method is valid for any all-pole transfer function, which is initially implemented with a commensurate-line distributed unit element prototype. The impulse response of that initial prototype is then properly interpolated to obtain the target response for a smooth-profiled filter with similar length and profile excursion. Finally, the target impulse response just generated is implemented in the rectangular waveguide technology employing a novel inverse scattering synthesis technique that relies on the coupled-mode theory to model the electromagnetic behavior of the waveguide filter. The novel inverse scattering synthesis technique is general and also valid for the case of filters with very high rejection levels, which is of great relevance in rectangular waveguide technology. A Ku-band low-pass filter with stringent satellite specifications is designed using the proposed method, fabricated by means of a direct metal AM technique, and measured with a vector network analyzer. A very good agreement is achieved between the simulated and measured results, fulfilling the required specifications and demonstrating the feasibility and performance of the novel design method.**

***Index Terms*— Additive manufacturing (AM), coupled-mode theory, filter synthesis, inverse scattering, microwave filter, rectangular waveguide.**

Manuscript received 29 December 2022; accepted 16 January 2023. Date of publication 28 February 2023; date of current version 30 June 2023. This work was supported in part by the Spanish Ministerio de Ciencia e Innovación—Agencia Estatal de Investigación (MCIN/AEI/10.13039/501100011033) under Project TEC2017-85529-C3-2-R (co-funded by the Fondo Europeo de Desarrollo Regional (FEDER) "A way to make Europe") and Project PID2020-112545RB-C53, and in part by the Advanced Technologies for future European Satellite Applications (TESLA) Project (European Union's Horizon 2020 Research and Innovation Programme through the Marie Sklodowska-Curie Grant) under Grant 811232. *(Corresponding author: Jabir Hussain.)*

Jon M. Percaz, Jabir Hussain, Ivan Arregui, Fernando Teberio, David Benito, Israel Arnedo, Miguel A. G. Laso, and Txema Lopetegi are with the Institute of Smart Cities (ISC), Department of Electrical, Electronic and Communications Engineering, Public University of Navarre (UPNA), Campus Arrosadia, 31006 Pamplona, Spain (e-mail: jabir.hussain@unavarra.es).

Petronilo Martin-Iglesias is with the European Space Research and Technology Centre, European Space Agency (ESTEC-ESA), 2201 AZ Noordwijk, The Netherlands.

Color versions of one or more figures in this article are available at https://doi.org/10.1109/TMTT.2023.3245683.

Digital Object Identifier 10.1109/TMTT.2023.3245683

I. Introduction

ADDITIVE manufacturing (AM) was developed in the 1980s to be employed in a large number of applications. Several manufacturing technologies can be included within the AM category, where the main distinctive feature is to build the objects by adding material (layer by layer) instead of machining raw material blocks in a subtractive process [such as the widely used computer numerical control (CNC) milling] [1], [2], [3], [4].

AM offers a great variety of possible base materials: plastics, ceramics, or metals. Specifically, the selective laser melting (SLM) technology produces all-metal components from metallic powders by stacking layers of these materials on top of each other. The potential of this fabrication technique is considerable since it permits the manufacturing of monolithic metal components with complex geometries and good mechanical and thermal properties, such as tensile strength, stiffness, wide working temperature range, and good thermal conductivity and thermal expansion properties. At the same time, SLM, as the other AM technologies, allows us to build complex devices that can even include several "assembled components," reducing waste, material, mass, envelope, interface flanges, lead/assembly time, test procedures, and cost [5], [6]. In spite of these advantages, it has not been until the last years when SLM has attracted the interest for the design of microwave components and when it has achieved enough maturity to be considered for the fabrication of waveguide filters [6], [7], [8], [9], [10], [11]. Nevertheless, very interesting progress has been made in recent times, including the qualification of SLM-manufactured Ku-band filters for space applications [12] and a demonstration of the integration of several RF functionalities, among which is filtering, in a single waveguide component exploiting the free-form capabilities provided by SLM [13].

However, there are still several challenges that need to be addressed in this technology for the implementation of microwave filters, such as the tolerances and surface roughness achieved, and the reproducibility obtained when several prototypes are fabricated [14]. In order to improve tolerances and surface roughness, it is necessary to carefully determine an adequate growing direction for the filter, as well

as to understand the internal stresses and possible associated shrinkage linked to the thermal issues that occur during the fabrication process [6], [15]. Surface roughness can be subsequently improved with postprocessing, through shot-peening of the inner surfaces and polishing of the flanges, achieving effective conductivities when employing AlSi10Mg alloy that can be satisfactory for many applications, and even silver coating can be finally applied if filters with very high Q are required [6], [13], [16], [17], [18]. Moreover, it is essential to always maintain the same building conditions (growing direction, support structures, machine parameters, etc.) to achieve high reproducibility levels. In order to deal with these concerns, several works have been recently proposed. In [15] and [16], step-shaped geometries are initially employed for the design of rectangular waveguide filters, showing the necessity of using support structures attached to the building platform to sustain overhanging surfaces. Indeed, due to the high thermal stresses arising in the SLM fabrication process, which can produce deformations, downward facing or sloping surfaces that form small angles with the horizontal plane of the building chamber have to be supported [19]. It is widely considered that downward sloping surfaces with angles larger than 45° are self-supporting, and the experimental results reported in [19] show that angles up to 30° can be built without supports, in both AlSi10Mg and Ti6Al4V alloys, using SLM. Thus, in order to fabricate the step-shaped geometries initially proposed in [15] and [16], the prototype was oriented in the building chamber with the filter propagation axis forming an adequate angle with the chamber vertical (building/growing) direction. The specific orientation angles were obtained following the study presented in [19], leading to self-supporting surfaces for the internal areas of the filter (where supports cannot be employed) so that support structures are only used for the external surface. An insightful analysis is performed in these last articles [15], [16], [19], and in others like [20], to show the importance of determining a suitable orientation angle to try to improve the fabrication tolerances and surface roughness of a specific device, revealing also the difficulty, resources, and postprocessing required to obtain good results when support structures are needed.

A very interesting strategy to enhance the manufacturing accuracy of SLM is to conceive AM-oriented filter topologies or design procedures that produce waveguide profiles that can be manufactured aligning the filter propagation axis with the building chamber vertical direction. This requires that all the downward sloping surfaces of the internal areas of the filter are self-supporting with that vertical alignment. To achieve it, in [15] and [16], the composite step/stub resonators of the filter have been tilted downward 45°. By using this optimum vertical building orientation, the classical SLM staircase effects are reduced, leading to lower surface roughness. Actually, the cross-sectional errors in the waveguide transversal plane will not be coupled with the longitudinal ones mainly related to the layer thickness. Thus, the accuracy of the waveguide cross section will depend on the laser beam-spot size and material shrinkage, and the profile along the propagation axis will be affected only by the staircase discretization due to the layer thickness, achieving optimum manufacturing accuracy [6], [15], [16], [21].

In order to enhance the performance of additive manufactured waveguide filters, the use of super-ellipsoid cavities and hyperbolic blended circular/elliptic irises was proposed in [12] and [22], obtaining rounded geometries. Although supports and oblique orientation were still needed to fabricate those filters, the authors recognized that the rounded shape of the filters made them easier to manufacture with SLM than conventional designs [12], [22]. Later, Booth [23] continued using rounded geometries, but proposing an AM-oriented design in the lines of [15] and [16], which can be fabricated aligning the filter propagation axis with the vertical building direction. Following this approach of using rounded surfaces and AM-oriented designs, lollypop-shaped resonators (spheres balanced on top of poles) have been proposed in [24] to implement stepped impedance resonators for bandpass filters. The resulting structure can be built along the vertical axis (the direction of the lollypop-shaped resonators) without the need of supports.

However, in all the previous references, the classical filter design methods employed for conventional structures (with step-shaped geometries) were used for the new smooth-shaped filters, which is not convenient for various reasons, primary being the requirement of long optimization processes that are especially inadvisable with rounded profiles. Therefore, it could be of great interest to conceive a filter synthesis technique that directly obtains devices with smooth profiles that can be always manufactured with the propagation axis oriented in the vertical building direction and with no need of electromagnetic optimization. In this way, the manufacturing accuracy of SLM will be optimized with the vertical building orientation, as it was previously explained, and with the smooth-profiled geometries that are easier to manufacture and avoid the presence of sharp edges (which could not be accurately built with SLM [9], [25]). At the same time, the SLM fabrication process will be significantly simplified, avoiding the need of specific orientation angles and support structures.

In this article, a novel filter design methodology based on direct synthesis is proposed. The design method is oriented to direct metal AM through SLM and satisfies all the valuable properties explained in the previous paragraph. The novel technique is developed for smooth-profiled rectangular waveguide filters, but it could be extended to other waveguide technologies. As it will be shown, the method is general and also valid for the very interesting case of filters with very high rejection levels.

This article is organized as follows. In Section II, a procedure to implement the desired all-pole transfer function with a commensurate-line distributed unit element (UE) prototype is explained. Then, a method to properly interpolate its impulse response, preserving the frequency response up to the required value, is proposed in Section III. The smooth interpolated impulse response will correspond to a filter with smooth profile, with length and profile excursion similar to those of the initial prototype. Next, in Section IV, the coupled-mode

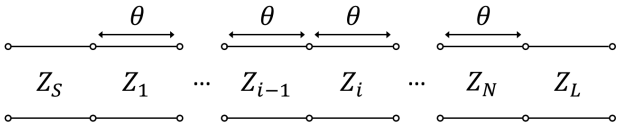

Fig. 1. Commensurate-line distributed prototype. Each line section has the same electrical length, θ, and different characteristic impedance, Z_i.

theory is employed to rigorously model the electromagnetic behavior of the smooth-profiled filter and, based on it, a novel inverse scattering synthesis technique is proposed valid for microwave filters with the interpolated impulse responses previously generated. Then, in Section V, to demonstrate the performance of the new filter design method oriented to direct metal AM, a Ku-band low-pass filter (LPF) with smooth profile and challenging satellite specifications is designed, fabricated, and measured in rectangular waveguide technology. Finally, the conclusions are drawn in Section VI.

II. Commensurate-Line Distributed UE Prototype

The first stage in the novel design procedure proposed in this article is to obtain a commensurate-line distributed prototype fulfilling the frequency specifications required for the filter. The prototype is formed by a cascade of N line sections, all of them with the same electrical length (commensurate) and different characteristic impedances, plus an additional input and output line section with the port impedances (see Fig. 1).

The synthesis of commensurate-line distributed networks (composed of commensurate lossless line sections and lumped resistors in general) can be formulated on an analogous basis to the synthesis of lumped-element networks by using the Richards' transformation [26], [27], [28]

$$t = \tanh\frac{a \cdot s}{2} \tag{1}$$

where the complex frequency (Laplace) variable s is transformed to a new complex variable t, and the constant $a = l/c$, i.e., it is the ratio between the length of a commensurate line, l, and the velocity of propagation of electromagnetic waves in the line, c. Using the Richards' transformation, the driving-point impedance of a commensurate distributed network, as well as the parameters of its scattering, transfer, and immittance matrices, can be expressed as rational functions in t [26], [27], [28]. The use of the half-argument $a \cdot s/2$ in the hyperbolic tangent in (1) is required so that the transmittances become rational functions in t. However, if the full argument $a \cdot s$ is employed, the driving-point impedance and all the matrix parameters remain rational functions in t, except for the possible appearance of irrational factors of the form $(1-t^2)^{1/2}$ in the transmittances [27], [28], [29]. In this case, the Richards' transformation is defined as

$$t = \tanh(a \cdot s) \tag{2}$$

and the degree of the rational functions in t of the scattering, transfer, and immittance matrices, and of the driving-point impedance, is reduced by half when compared to the original transformation of (1). Actually, this last form of the Richards' transformation is preferred and used in the vast majority of books and articles published in the last decades [27], [28], [29], [30], [31], [32], [33], [34], [35], where expressions identical or equivalent to (2) are employed, and it will be used in this article.

As presented in (1) and (2), the Richards' transformation can be applied only to ideal transmission lines since a constant velocity of propagation c (not variable with frequency) is assumed in the definition of $a = l/c$. However, it can be easily extended to waveguides (where a phase velocity, v_p, variable with frequency must be considered), by introducing the concept of electrical length of the commensurate lines, $\theta = \beta \cdot l$, where $\beta = \omega/v_p$ is the phase constant of the waveguide operation mode, $\omega = 2\pi f$ is the frequency in rad/s, and f is the frequency in Hz [29], [35]. Thus, the Richards' transformation of (2) can be rewritten as [35]

$$t = \tanh(j\theta) = j \cdot \tan(\theta) \tag{3}$$

since the argument $j\theta = j\omega l/v_p = sl/v_p$, where $\omega = s/j$ is employed to perform the analytic continuation to the complex frequency plane, s.

Inspecting (2) and (3), it can be seen that the Richards' transformation maps the (imaginary) frequency axis ($j\omega$) of the complex frequency (Laplace) plane, s, to the (imaginary) frequency axis ($j\Omega$) of the Richards' transform plane, t, through the equation [27], [28], [30]

$$\Omega = \tan(\theta) \tag{4}$$

where

$$\theta = \beta l = \omega l/v_p \tag{5}$$

is the electrical length of the commensurate lines (either transmission or waveguide line sections). Therefore, the mapping between frequency axes is periodic in θ, and actually, all responses of commensurate distributed networks will be periodic with respect to θ (and to ω for the case of ideal transmission lines where v_p does not vary with frequency [27], [28], [31], [32], [33], [34]). Additionally, it can be demonstrated that the right half of the s-plane maps on the right half of the t-plane, while the left half s-plane maps on the left half t-plane. Consequently, the Richards' transformation behaves adequately preserving network realizability conditions and a positive real function of t has the same property with respect to s [27], [28].

The input impedance, in the Richards' transform plane, of a commensurate-line section (with electrical length θ and characteristic impedance Z_0) terminated in a short circuit is given by $Z_{sc} = Z_0 \cdot t$. In the same way, it can be easily demonstrated using (3) that the input impedance of a commensurate-line section terminated in an open circuit is $Z_{oc} = Z_o/t$. Therefore, a short-circuited stub and an open-circuited stub behave, in the Richards' transform plane, as a lumped inductor and a lumped capacitor, respectively [27], [28], [29], [30], [31], [32], [34], [35]. However, a commensurate-line section (with electrical length θ and characteristic impedance Z_0), viewed as a two-port, has no lumped-element counterpart and is termed UE [27], [28], [29], [30], [31], [32], [33], [34], [35]. Its transfer matrix in the t-plane is [28], [29], [31], [32], [34], [35]

$$\begin{bmatrix} A & B \\ C & D \end{bmatrix}_{UE} = \frac{1}{\sqrt{1-t^2}} \begin{bmatrix} 1 & Z_0 t \\ t/Z_0 & 1 \end{bmatrix}. \tag{6}$$

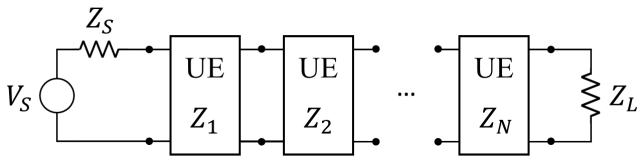

Fig. 2. Commensurate-line distributed prototype represented in the Richards' transformation domain as a cascade of N UEs.

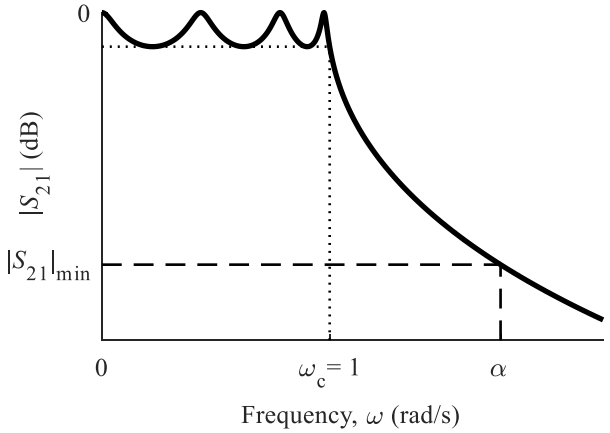

Fig. 3. Frequency response of the normalized all-pole Chebyshev function taken as example. The transmission value obtained at $\omega = \alpha$ is labeled $|S_{21}|_{min}$ since it will correspond to the minimum transmission (maximum attenuation) achieved by the commensurate-line distributed prototype.

Let us focus now on the commensurate-line distributed prototype of interest for the novel design method proposed in this article. It is formed by a cascade of N line sections, all of them with the same electrical length and different characteristic impedances, with an additional input and output line section with the port impedances (see Fig. 1). Therefore, in the Richards' transformation domain, it can be modeled as a cascade of N UEs, plus the input and output ports (see Fig. 2). By multiplying the transfer matrices of the N UEs, it can be demonstrated that the transmission coefficient (S_{21} parameter) of a lossless two-port network obtained by cascading N UEs, as shown in Fig. 2, satisfies [28], [29], [35]

$$S_{21}(t) = \frac{\left(1 - t^2\right)^{N/2}}{P_N(t)} \tag{7}$$

where $P_N(t)$ is a strictly Hurwitz polynomial in t of order N (a polynomial with real positive coefficients and all its roots in the open left half plane, $\mathrm{Re}(t) < 0$), and $|S_{21}(t = j\Omega)| \leq 1$.

Inspecting (6) and (7), it can be seen that each UE produces a half-order transmission zero at $t = \pm 1$. Other transmission zeros (even at infinity) are not possible with this structure [27], [35]. Therefore, in order to implement the classical all-pole functions (Butterworth, Chebyshev, Zolotarev, ...), which have all the transmission zeros at infinity, a mapping must be first applied to move all the transmission zeros of the all-pole function from $s = \pm j\infty$ to $t = \pm 1$ [35]. Starting from the normalized all-pole transfer function [with cutoff frequency $\omega_c = 1$ rad/s (see Fig. 3)], the following mapping function is applied:

$$\omega = \frac{\sin\theta}{\sin\theta_c} = \alpha \cdot \sin\theta \tag{8}$$

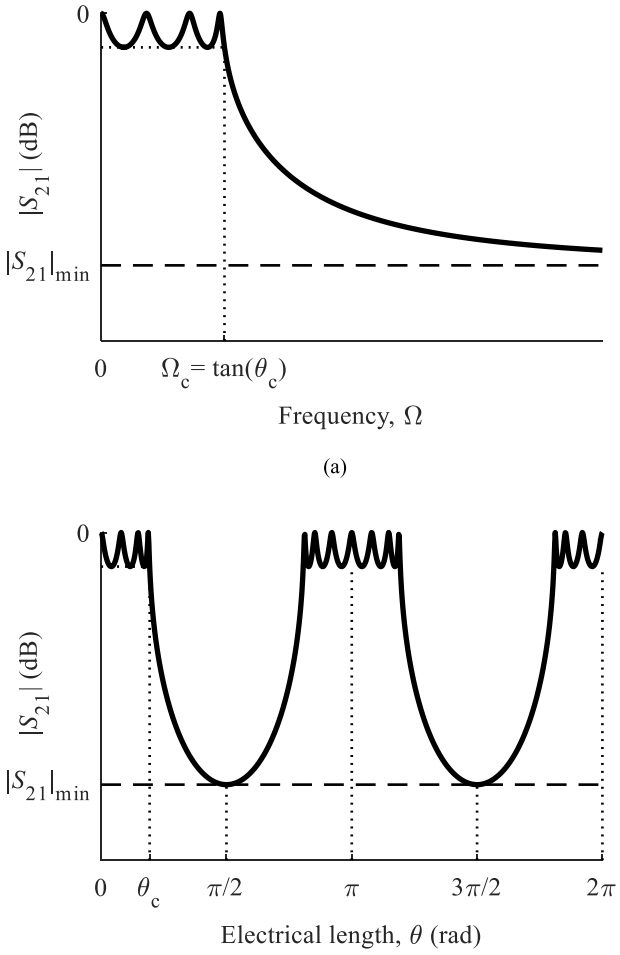

Fig. 4. Frequency response of the commensurate-line distributed UE prototype of Figs. 1 and 2 for the all-pole Chebyshev function taken as example of Fig. 3: (a) $|S_{21}|$ in the Richards' transform domain, as a function of the frequency axis $t = j\Omega$ and (b) $|S_{21}|$ in the natural frequency domain, as a function of the electrical length of the commensurate lines (or UEs), θ.

where θ_c is the electrical length of the commensurate lines at the filter cutoff frequency and $\alpha = 1/\sin\theta_c$. Then, the Richards' transformation is employed in the form of (3), and using $\omega = s/j$ to perform the analytic continuation to the complex frequency plane s and taking advantage of the identity $\sin\theta = \tan\theta/\sqrt{1 + \tan^2\theta}$, it results [35]

$$s = \frac{\alpha \cdot t}{\sqrt{1 - t^2}} \tag{9.a}$$

$$t = \frac{\pm s}{\sqrt{\alpha^2 + s^2}}. \tag{9.b}$$

As it can be seen, by changing the complex frequency variable s of the all-pole transfer function $S_{21}(s) = 1/P'_N(s)$ to t using (9.a), the half-order transmission zeros at $t = \pm 1$ are introduced, replacing the original transmission zeros at infinity and obtaining a transfer function of the form of (7) as intended [35]. The order of the all-pole transfer function, N, is equal to the number of UEs required for the filter implementation.

The resulting frequency responses are shown in Fig. 4 for the all-pole Chebyshev function taken as example. The frequency responses are given in the Richards' transform

domain (in the frequency axis $t = j\Omega$), and in the natural frequency domain (as a function of the electrical length of the commensurate lines, θ), with both frequency axes related through (4). Additionally, they are related to the normalized frequency response of Fig. 3 through (8). As it can be seen, the passband characteristics are identical to those of the normalized frequency response of Fig. 3 (equiripple responses with identical ripple levels in our Chebyshev case), with a cutoff frequency of $\Omega_c = \tan(\theta_c)$ in the Richards' domain and θ_c in the natural frequency domain (electrical length axis). Moreover, the maximum attenuation (minimum transmission $|S_{21}|_{\min}$) is achieved for $\Omega \longrightarrow \infty$ (in the Richards' domain) and for $\theta = \pi/2$ (in the natural frequency domain). The maximum attenuation value is equal to the attenuation of the normalized all-pole transfer function at the frequency $\omega = \alpha = 1/\sin\theta_c$ (see (8) and Fig. 3). Beyond $\theta = \pi/2$, the frequency response repeats periodically [as indicated by (4), taking into account that the frequency responses will have Hermitian symmetry, $S_{21}(-\Omega) = S_{21}^*(\Omega)$], and it happens in any commensurate distributed network. Equivalent methods to implement all-pole functions using commensurate-line distributed prototypes of the form of Fig. 1 are proposed in [27], [28], [29], and [36], relying all of them on mapping functions of the form of (8).

Once the required transfer function in the Richards' transform plane, $S_{21}(t)$, fulfilling (7) is chosen, the values (characteristic impedances) of the UEs that form the commensurate-line distributed prototype (see Fig. 2) can be calculated. Different methods can be employed to perform the calculations. The first method is based on the iterative application of the Richards' theorem, which allows us to extract the UEs sequentially from the input impedance of the network, leaving a remainder impedance after each extraction [27], [28], [34]. The second method is easier to program and is based on the iterative extraction of the UEs from the transfer matrix [*ABCD*] of the network, leaving a remainder transfer matrix after each extraction [35]. The values of the UEs can also be calculated using commercial software tools, like Keysight Genesys S/Filter or Filsyn.

III. Modification of the UE Prototype Response to Produce a Filter With Smooth Profile

In Section II, a commensurate-line distributed UE prototype has been obtained fulfilling the required frequency specifications. The prototype is formed by a cascade of N line sections, all of them with the same electrical length and different characteristic impedances (see Fig. 1). From this stepped-impedance prototype, a filter with smooth profile will be obtained, retaining a similar length and profile excursion to those of the original commensurate-line distributed UE prototype. To do it, the UE prototype response will be carefully modified exploiting properties of the relationship between the impulse response and the frequency response of a linear time-invariant device. In order to ease the explanation of the followed procedure, we will start with the simplest case where the filter is implemented in ideal transmission line technology. Next, the more complex case of implementation in waveguide technology will be studied.

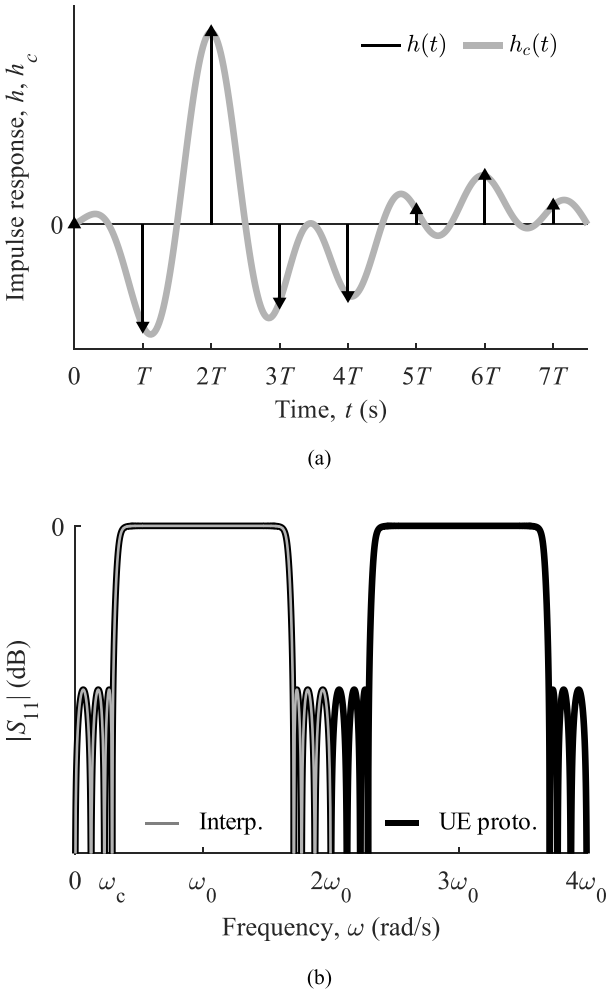

Fig. 5. Responses in the time and frequency domains for the case of ideal transmission line: (a) impulse response in reflection of the UE prototype, $h(t)$, formed by a sequence of equidistant impulses, and underlying continuous impulse response, $h_c(t)$, obtained by performing an ideal bandlimited interpolation with $m = 2$ and (b) frequency response in reflection of the UE prototype periodic in ω, and frequency response corresponding to the continuous impulse response $h_c(t)$ obtained by performing an ideal bandlimited interpolation with $m = 2$.

A. Implementation in Ideal Transmission Line Technology

In this case, the phase velocity v_p does not vary with frequency, and it represents the propagation velocity along the line sections of the UE prototype. All the commensurate (same electrical length) line sections will have the same physical length l [see (5)], and the propagation time through a line section will be l/v_p. Therefore, the impulse response, $h(t)$, of the UE prototype [the time-domain response to an impulse or Dirac delta function, $\delta(t)$] will be an impulse train formed by a sequence of equidistant impulses separated T seconds apart [see Fig. 5(a)]

$$h(t) = \sum_{n=0}^{\infty} a_n \cdot \delta(t - nT) \tag{10}$$

where $T = 2 \cdot l/v_p$ is the time taken by the impulse to go through a line section, multiplied by 2. Please note that in this section t is used as the time variable. The form of the impulse response given in (10) is valid for the transmission and reflection responses of the UE prototype, and it can be easily verified by "following" the propagation of the input impulse

$\delta(t)$ through the UE prototype, as it reflects and transmits at the junctions between the line sections with different characteristic impedances (see Fig. 1). The transmission impulse response would also include an initial propagation delay. The coefficients of the impulses in (10), a_n, could be seen as samples of an underlying continuous impulse response, $h_c(t)$, multiplied by T for convenience as

$$a_n = h_c(t = nT) \cdot T. \tag{11}$$

In this way, the frequency response of the UE prototype, $H(\omega)$, can be expressed as a periodic replication and superposition of the frequency response corresponding to the underlying continuous impulse response, $H_c(\omega)$ [37], [38]

$$H(\omega) = \sum_{n=-\infty}^{\infty} H_c(\omega + 2\omega_0 n) \tag{12}$$

where

$$\omega_0 = \frac{\pi}{T}. \tag{13}$$

Actually, as it is shown in Fig. 5(b) for $S_{11}(\omega)$, the frequency response of the UE prototype will be periodic in ω since it is periodic in θ [see Fig. 4(b)], and the constant v_p and l of our transmission line case will make it also periodic in ω [see (5)]. Thus, the frequency response of the UE prototype can be seen indeed as the periodic replication and superposition of (12).

Additionally, by applying the sampling theorem [37], performing an ideal bandlimited interpolation of the UE prototype impulse response of (10), the underlying continuous $h_c(t)$ [see Fig. 5(a)], can be calculated as [37], [38]

$$h_c(t) = \sum_{n=-\infty}^{\infty} a_n \cdot \frac{\sin(\omega_{\max}(t - nT))}{\pi(t - nT)} \tag{14}$$

where $\omega_{\max}$ is the maximum frequency of the interpolated impulse response, $h_c(t)$, in the sense that its frequency response, $H_c(\omega)$, is equal to $H(\omega)$ up to $\omega_{\max}$, and zero beyond that frequency. In the classical ideal bandlimited interpolation, $\omega_{\max} = \pi/T = \omega_0$ [37], [38]. However, in our case of interpolating the UE prototype impulse response, $h(t)$, to obtain a continuous $h_c(t)$ to synthesize a filter with smooth profile, it is possible and more convenient to take $\omega_{\max} = m \cdot \omega_0$, with m integer, where $m = 2$ will be used to implement an LPF [see Fig. 5(b)], and $m = 4$ could be taken to implement a bandpass filter. The introduction of the m factor in $\omega_{\max}$ can be compensated in (14) simply by introducing the same factor in a_n as

$$a_n = h_c(t = nT) \cdot T/m. \tag{15}$$

As it will be shown in Section IV, the inverse scattering synthesis method that will be employed to obtain the filter with smooth profile will start from the target filter response in reflection defined by the Fourier transform pair

$$\begin{aligned} F(\tau) &\longleftrightarrow S_{11}(\beta) \\ F(\tau) &= \frac{1}{2\pi} \int_{-\infty}^{\infty} S_{11}(\beta) \cdot e^{j\beta\tau} \cdot d\beta \end{aligned} \tag{16}$$

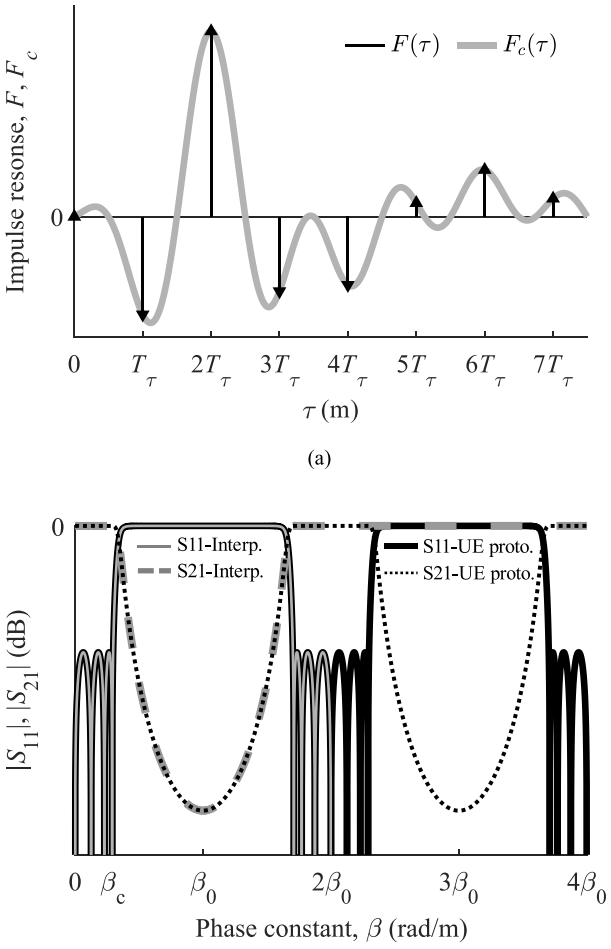

Fig. 6. Responses in the τ and β domains for the cases of ideal transmission line and rectangular waveguide: (a) impulse response in reflection of the UE prototype, $F(\tau)$, formed by a sequence of equidistant impulses, and underlying continuous impulse response, $F_c(\tau)$, obtained by performing an ideal bandlimited interpolation with $m = 2$ and (b) frequency response of the UE prototype periodic in β, and frequency response corresponding to the continuous impulse response $F_c(\tau)$ obtained by performing an ideal bandlimited interpolation with $m = 2$: in reflection,$|S_{11}|$ parameter, and in transmission, $|S_{21}|$ parameter.

where $F(\tau)$ is the inverse Fourier transform of the $S_{11}(\beta)$ parameter (frequency response in reflection as a function of the phase constant, β). For the case studied in this section of ideal transmission line technology (phase velocity, v_p, constant with frequency), a simple and direct relationship can be established between the Fourier transform pair of (16) and the classical time–frequency pair. Actually, by applying the Fourier transform property of time and frequency scaling [37], [39], it can be obtained

$$v_p \cdot F(v_p \cdot t) \longleftrightarrow S_{11}\left(\frac{\omega}{v_p}\right) \tag{17}$$

since $\beta = \omega/v_p$ and v_p is a positive real constant. Therefore, the impulse response in reflection will satisfy $h(t) = v_p \cdot F(v_p \cdot t)$ and $\tau = v_p \cdot t$, and from (10), it can be deduced that the impulse response of the UE prototype in the τ domain will have the form [see Fig. 6(a)]

$$F(\tau) = \sum_{n=0}^{\infty} a_n \cdot \delta(\tau - nT_\tau) \tag{18}$$

since $\delta(v_p \cdot t) = \delta(t)/v_p$, where $T_\tau = v_p \cdot T$

$$T_\tau = 2 \cdot l \tag{19}$$

being l the physical length of the commensurate-line sections of the UE prototype. Additionally, by employing the relationships that we have just obtained, the ideal bandlimited interpolation of (14) can be rewritten for $F(\tau)$ as [see Fig. 6(a)]

$$F_c(\tau) = \sum_{n=-\infty}^{\infty} a_n \cdot \frac{\sin(\beta_{max}(\tau - nT_\tau))}{\pi(\tau - nT_\tau)} \tag{20}$$

where

$$\beta_{max} = m \cdot \beta_0 \tag{21}$$

with m integer and $\beta_0 = \omega_0/v_p$ defined from (13) as

$$\beta_0 = \frac{\pi}{T_\tau} \tag{22}$$

and the coefficients of the impulses in (18), a_n, satisfying a similar relationship to that of (15)

$$a_n = F_c(\tau = nT_\tau) \cdot T_\tau/m. \tag{23}$$

Thus, by interpolating the impulse response in reflection of the UE prototype of (18), $F(\tau)$, as shown in (20), a continuous $F_c(\tau)$ is obtained to synthesize a filter with smooth profile whose frequency response in reflection, $S_{11,c}(\beta)$, is identical to that of the UE prototype up to $\beta_{max} = m \cdot \beta_0$, and zero beyond that frequency (see Fig. 6). The coefficients of the impulses in (18), a_n, are equal to those of (10) (identical impulse coefficients in the time and τ domains), and they can be readily calculated from the characteristic impedances of the UE prototype, Z_i, following the procedure explained in the Appendix.

B. Implementation in Rectangular Waveguide Technology

In the case of rectangular waveguide technology, the fundamental TE_{10} mode will be employed, keeping the width of the waveguide constant and varying its height along the device. In this way, the phase constant, β, will not vary along the filter and will remain constant for a given frequency [40]. Consequently, the frequency response of the UE prototype that is periodic in θ [see Fig. 4(b)] will also be periodic in β, as it can be easily deduced from (5), with all the line sections having the same physical length, l. Thus, the frequency response of the UE prototype will have the form of Fig. 6(b) and can be seen as a periodic replication and superposition in β of the form of (12), where ω is substituted by β

$$S_{11}(\beta) = \sum_{n=-\infty}^{\infty} S_{11,c}(\beta + 2\beta_0 n). \tag{24}$$

Therefore, the impulse response in reflection of the UE prototype in the τ domain, $F(\tau)$, will have the form of Fig. 6(a), with an expression given by (18) and (19), where the coefficients of the impulses, a_n, can be seen as samples of an underlying continuous impulse response, $F_c(\tau)$, satisfying (23). By applying the ideal bandlimited interpolation of (20), a continuous impulse response $F_c(\tau)$ is obtained [see Fig. 6(a)], corresponding to a rectangular waveguide filter with smooth profile. The resulting filter will have a length and profile excursion similar to those of the UE prototype, with a frequency response $S_{11,c}(\beta)$ identical to that of the UE prototype up to β_{max}, and zero beyond that frequency. The value of β_{max} is fixed through (21) and (22), where $\beta_{max} = 2 \cdot \beta_0$ is taken to implement an LPF ($m = 2$), and $\beta_{max} = 4 \cdot \beta_0$ could be used to implement a bandpass filter ($m = 4$) [see Fig. 6(b)]. The introduction of the m factor in β_{max} must be formally compensated in (24) by introducing a $1/m$ factor on the right-hand side of the equation.

As it can be seen, the equations employed to modify the UE prototype response to subsequently synthesize a filter with smooth profile are identical in the case of rectangular waveguide and ideal transmission line. This is due to the fact that both technologies produce UE prototypes with frequency responses $S_{11}(\beta)$ periodic in β, and impulse responses $F(\tau)$ formed by a sequence of equidistant impulses in τ, which can be interpolated using the same procedure and equations. In the same way, the coefficients of the impulses of $F(\tau)$, a_n, can be calculated from the Z_i's of the UE prototype as explained in the Appendix, using also identical procedures for the case of rectangular waveguide and for ideal transmission line. However, it is interesting to note that the expressions for the impulse response in the time domain (10), the frequency response in the frequency domain ω (12), and of course the interpolation in the time domain (14) are not valid for rectangular waveguide technology due to its inherent dispersion (phase velocity v_p variable with frequency). However, the corresponding expressions in the τ and β domains are indeed valid as it has been demonstrated above, and they will be the equations employed for our inverse scattering synthesis procedure.

IV. Synthesis Technique for Rectangular Waveguide Filters With Smooth Profile and High Rejection

In Sections II and III, a procedure to implement any all-pole transfer function with a commensurate-line distributed UE prototype has been explained (Section II), and then, a method to properly interpolate its impulse response in the τ domain has been proposed, keeping the frequency response unaltered up to a chosen β_{max} (Section III). The interpolated (smooth) impulse response will correspond to a filter with smooth profile, with length and profile excursion similar to those of the initial UE prototype. In order to implement the smooth profiled filter in the rectangular waveguide technology, the electromagnetic behavior of the device will be rigorously modeled through the coupled-mode theory (as explained in Section IV-A) and a suitable inverse scattering synthesis technique will be applied to obtain the required modal coupling coefficient to implement the target filter response (as it will be shown in Section IV-B). Several inverse scattering synthesis methods for microwave devices have been reported in the past (see [41], [42], [43]). Unfortunately, none of them allows us to implement the modified responses (interpolated in the τ domain) obtained in Section III for smooth profiled filters, when very high rejection

levels are required. Since very high rejection levels are a common design specification for rectangular waveguide filters, inspired by a method developed in the optics field for fiber Bragg gratings with very high reflectivity [44], a new inverse scattering synthesis technique will be proposed and employed in this article, which is also valid for microwave filters having very high rejection levels as design specifications (see details in Section IV-B).

A. Coupled-Mode Theory: Application to Rectangular Waveguide With Symmetrical Variations in Height

In order to obtain an accurate coupled-mode formulation for our nonuniform rectangular waveguide devices, we will take advantage of the cross-sectional method. It allows us to describe the electromagnetic fields at any cross section of the nonuniform waveguide as a superposition of the fields of the orthogonal modes (taking into account their forward and backward traveling waves) corresponding to an auxiliary uniform waveguide characterized by the same cross-sectional dimensions and distribution of electrical permittivity, ε, and magnetic permeability, μ [45]. Assuming sinusoidal steady-state time dependence for the fields and using their phasor representation, the total electric and magnetic fields, $\vec{E}(x, y, z)$ and $\vec{H}(x, y, z)$, can be written as

$$\vec{E}(x, y, z) = \sum_i a_i(z) \cdot \vec{E}^i(x, y, z) \tag{25.a}$$

$$\vec{H}(x, y, z) = \sum_i a_i(z) \cdot \vec{H}^i(x, y, z) \tag{25.b}$$

where x, y are the coordinate axes of the rectangular waveguide cross section, z is the propagation direction axis, and $\vec{E}^i(x, y, z)$ and $\vec{H}^i(x, y, z)$ are the electric and magnetic vector mode patterns associated with the i mode, with $i > 0$ corresponding to a forward traveling wave and $i < 0$ to a backward traveling wave. Finally, $a_i(z)$ stands for the complex amplitude of the i mode along the nonuniform waveguide. It can be demonstrated that if the field decomposition of (25) is introduced into the Maxwell's equations, it will give rise to the so-called coupled-mode equations [45]

$$\frac{da_m}{dz} + j \cdot \beta_m \cdot a_m = \sum_i C_{mi} \cdot a_i \tag{26}$$

where C_{mi} is the coupling coefficient between the m and i modes, and β_m is the phase constant of the m mode that can be expressed (for $m > 0$) as [40], [42]

$$\beta_m = -\beta_{-m} = \sqrt{k^2 - k_{cm}^2} \tag{27}$$

being k the wavenumber of the dielectric medium that fills the waveguide, $k = \omega\sqrt{\mu\varepsilon}$, with $\omega = 2\pi f$, and k_{cm} the cutoff wavenumber of the m mode that can be calculated for our case of rectangular waveguide as [40]

$$k_{cm} = \sqrt{\left(\frac{\pi \cdot p_m}{a}\right)^2 + \left(\frac{\pi \cdot q_m}{b}\right)^2} \tag{28}$$

where a and b are the total width and height of the rectangular waveguide cross section of interest, while p_m and q_m are the modal indexes of the m mode.

Going back to the coupling coefficient, C_{mi}, of (26), a general expression to calculate it for our case of interest of a nonuniform waveguide with closed metallic contour of variable cross section can be written as [42], [45]

$$C_{mi} = \frac{-\pi \cdot f \cdot \oint \nu \cdot \left[\mu \cdot H_z^m \cdot H_z^i - \mu \cdot H_t^m \cdot H_t^i + \varepsilon \cdot E_n^m \cdot E_n^i\right] \cdot dt}{N_m \cdot (\beta_m - \beta_i)} \tag{29}$$

where the integration is carried out over the metallic contour of the cross section, using a local coordinate system with axes n, t, z defined as follows: n is normal and t is tangential to the metallic contour of the cross section, with both axes contained in the cross section, z is the propagation direction, and their unit vectors satisfy $\hat{n} \times \hat{t} = \hat{z}$, with $\hat{n}$ directed toward the metal. Moreover, $\nu = \tan(\alpha)$, being α the angle defined between the propagation direction, z, and the line tangential to the metal–dielectric interface of the nonuniform waveguide contained in the nz plane. Finally, N_m is the normalization factor of the m mode, $N_m = \iint_S (\vec{E}^m \times \vec{H}^m) \cdot d\vec{S}$, defined in the surface of the cross section, and $N_m \neq N_m(z)$ is customarily taken for convenience, resulting in $C_{mm} = -1/(2 \cdot N_m) \cdot dN_m/dz = 0$. Further details about the calculation of the coupling coefficients through (29) are given in [42].

The sign convention employed in [41] and [42] for the vector mode patterns associated with the m mode, i.e., $E_x^m = E_x^{-m}$, $E_y^m = E_y^{-m}$, $E_z^m = -E_z^{-m}$, $H_x^m = -H_x^{-m}$, $H_y^m = -H_y^{-m}$, and $H_z^m = H_z^{-m}$, will also be followed in this article, resulting in $N_m = -N_{-m}$. Inspecting (29) and taking advantage of the sign convention employed and of (27), very useful properties to ease the calculation of the coupling coefficients can be found

$$C_{mi} \cdot N_m = -C_{im} \cdot N_i \tag{30.a}$$

$$C_{mi} = C_{-m-i}. \tag{30.b}$$

Now, we are going to apply the general expression for the coupling coefficient of (29) to our case under study of nonuniform rectangular waveguides with symmetrical variations in height. The details to perform the calculations are explained in [42]. Taking advantage of the analytical expressions available for the vector mode patterns of the TE and TM modes of the rectangular waveguide [40], analytical expressions for the coupling coefficients will also be obtained. The expressions for the required coupling coefficients can be greatly simplified by considering our case of interest where the rectangular waveguide structure with symmetrical variations in height is exclusively excited with the fundamental TE_{10} ($p_{m=1} = 1$ and $q_{m=1} = 0$) mode at the input port. In that case, only the $TE_{p_m q_m}$ and $TM_{p_m q_m}$ modes with indexes $p_m = 1$ and $q_m = 0, 2, 4, 6, \ldots$ can be excited within the structure since to get a nonnull coupling coefficient, $C_{mi} \neq 0$, the first modal indexes must be equal, $p_m = p_i$, while the second modal indexes must be of the same parity, i.e., $q_m + q_i$ must be an even number [42], [45]. Taking into account these considerations, the following expressions are obtained for the relevant coupling coefficients in our case under study

(between modes TE_{10}, TE_{12}, TE_{14}, TE_{16}, ... and TM_{12}, TM_{14}, TM_{16}, ...):

$$C_{m,\pm i}^{\mathrm{TE-TE}} = \frac{r_m r_i[(ak_{cm}k_{ci})^2 + \pi^2(\pm\beta_m\beta_i - k^2)]\sqrt{N_i}}{4(\beta_m \mp \beta_i)\sqrt{\beta_m}\sqrt{\beta_i}a^2 b(z)k_{cm}k_{ci}\sqrt{N_m}} \cdot \frac{db(z)}{dz} \tag{31.a}$$

$$C_{m,\pm i}^{\mathrm{TE-TM}} = \frac{\pm\pi^2 k r_m q_i \sqrt{N_i}}{2\sqrt{\beta_m}\sqrt{\beta_i}ab(z)^2 k_{cm}k_{ci}\sqrt{N_m}} \cdot \frac{db(z)}{dz} \tag{31.b}$$

$$C_{m,\pm i}^{\mathrm{TM-TM}} = \frac{\pi^2 q_m q_i(\pm k^2 - \beta_m\beta_i)\sqrt{N_i}}{(\beta_m \mp \beta_i)\sqrt{\beta_m}\sqrt{\beta_i}b(z)^3 k_{cm}k_{ci}\sqrt{N_m}} \cdot \frac{db(z)}{dz} \tag{31.c}$$

where $C_{m,i}^{\mathrm{TE-TE}}$, $C_{m,i}^{\mathrm{TE-TM}}$, and $C_{m,i}^{\mathrm{TM-TM}}$ are the coupling coefficients between two TE modes, between TE and TM modes and between two TM modes, respectively, and $r_m = \sqrt{2}$ for $TE_{p_m q_m}$ modes with modal indexes $p_m = 0$ or $q_m = 0$, whereas $r_m = 2$ otherwise. The coupling coefficient between TM and TE modes, $C_{m,i}^{\mathrm{TM-TE}}$, can be immediately obtained from $C_{m,i}^{\mathrm{TE-TM}}$ by applying the property (30.a).

It is important to note that $m > 0$ and $i > 0$ must be employed in (31.a)–(31.c). The couplings between the forward traveling waves ($m > 0$ and $i > 0$) will be considered by choosing the upper signs of these expressions, while the couplings between the forward traveling waves ($m > 0$) and the backward traveling waves ($i < 0$) will be determined by selecting the lower signs of the equations. The remaining coupling coefficients that concern the backward traveling m waves ($m < 0$) will be deduced from the application of property (31.b) to the expressions of $C_{m,\pm i}^{\mathrm{TE-TE}}$, $C_{m,\pm i}^{\mathrm{TE-TM}}$, and $C_{m,\pm i}^{\mathrm{TM-TM}}$ of (31.a)–(31.c).

Finally, it must be highlighted that the coupling coefficient expressions of (31) determine the electromagnetic behavior of a nonuniform rectangular waveguide that exhibits symmetrical variations in its height, when it is excited with the fundamental TE_{10} mode. Once the coupling coefficients, C_{mi}, are known, the coupled-mode equations of (26) can be solved for each m mode just by imposing the following boundary conditions: $a_1(z=0) = 1$ and $a_m(z=0) = 0$ for all $m \neq 1$, which means that the structure is being excited at the input port with the forward traveling wave of the fundamental TE_{10} mode and $a_m(z = L) = 0$, with $m \leq -1$, which implies that the waveguide structure of length L is loaded at the output port with a perfect matched load. This procedure will allow us to calculate the complex amplitude of each m mode, $a_m(z)$, along the nonuniform rectangular waveguide [see (25) and (26)], for all the relevant modes, in our case: TE_{10}, TE_{12}, TE_{14}, TE_{16},... and TM_{12}, TM_{14}, TM_{16}, ..., including their forward and backward traveling waves. Additionally, it allows us to obtain the S-parameters of the device immediately as: $S_{11} = a_{-1}(z = 0)$ and $S_{21} = a_1(z = L)$.

1) Single-Mode Operation: Once the general coupled-mode theory has been carefully formulated for our case of nonuniform rectangular waveguide devices that feature symmetrical variations in height, a useful approximation can be done by considering that the operation frequency range of the device will be always within the single-mode regime, where only the fundamental TE_{10} mode is in propagation and all the higher order modes are under cutoff. Thus, if we consider only the fundamental mode and neglect the parasitic contributions of cutoff modes in (26), the single-mode coupled-mode equation system is obtained

$$\frac{da^+}{dz} = -j \cdot \beta \cdot a^+ + K \cdot a^- \tag{32.a}$$

$$\frac{da^-}{dz} = j \cdot \beta \cdot a^- + K \cdot a^+ \tag{32.b}$$

where a^+ and a^- are the complex amplitudes of the forward (+) and backward (−) traveling waves of the fundamental TE_{10} mode along the nonuniform waveguide, K is the coupling coefficient between both waves, i.e., $K = C_{1,-1} = C_{-1,1}$, β is the phase constant of the TE_{10} mode, and z is the propagation direction. An expression for $K = C_{1,-1}$ can be readily obtained from (31.a), resulting in

$$K(z) = -\frac{1}{2 \cdot b(z)} \cdot \frac{db(z)}{dz}. \tag{33}$$

As it can be seen, the coupling coefficient, $K(z)$, depends only on the waveguide height profile, $b(z)$. Therefore, if we are able to determine the coupling coefficient required to obtain a target frequency response, it will suffice to calculate the waveguide height profile that corresponds to that coupling coefficient, in order to synthetize the rectangular waveguide device that meets the target frequency response. The waveguide height profile, $b(z)$, for a certain $K(z)$ can be deduced from (33) as

$$b(z) = b(0) \cdot e^{-2 \cdot \int_0^z K(r) \cdot dr} \tag{34}$$

where $b(0)$ is the height at $z = 0$ (input port), which can be arbitrarily chosen.

However, it must be noticed that if we analyze the frequency response of the fundamental mode ($m = \pm 1$) of a nonuniform waveguide structure, considering also the higher order modes that are under cutoff, i.e., solving (26), the results will be slightly different from the single-mode operation approximation defined by the equation system (32). This discrepancy is due to the parasitic reactive couplings between the fundamental and the cutoff modes, which are taken into account in the general form of the coupled-mode equations (26), where all modes and their interactions are considered.

2) Approximation to Take Into Account the Effect of the Cutoff Modes: An approximation based on the general form of the coupled-mode equations of (26) will be proposed here, in order to take into account the effect of the cutoff modes when employing the single-mode coupled-mode equation system of (32) to perform the synthesis of microwave filters.

First, particularizing (26) for the case of $m = 1$ (forward traveling wave of the fundamental TE_{10} mode), its corresponding coupled-mode equation is obtained. Extracting the term associated with the backward traveling wave of the fundamental TE_{10} mode ($i = -1$) from the summation, the following expression will be reached

$$\frac{da_1}{dz} = -j \cdot \beta_1 \cdot a_1 + C_{1,-1} \cdot a_{-1} + \sum_{|i|>1} C_{1,i} \cdot a_i. \tag{35}$$

Comparing (35) with (32.a), it can be seen that both expressions are identical (except for the cutoff modes term) if the following identities are recalled: $C_{1,-1} = K$, $a_1 = a^+$, $a_{-1} = a^-$, and $\beta_1 = \beta$. Actually, a very useful rearrangement can be applied to the cutoff modes term of (35), yielding to

$$\frac{da_1}{dz} = -j \cdot \left(\beta_1 + j \cdot \sum_{|i|>1} \frac{C_{1,i} \cdot a_i}{a_1} \right) \cdot a_1 + C_{1,-1} \cdot a_{-1}. \quad (36)$$

Now, by inspecting (36), comparing it again with (32.a), it is clear that the parasitic effect of the higher order mode couplings can be interpreted as an effective modification of the propagation constant of the fundamental TE_{10} mode along the propagation direction. Indeed, we can introduce an effective complex propagation constant, β', leading to

$$\frac{da_1}{dz} = -j \cdot \beta' \cdot a_1 + C_{1,-1} \cdot a_{-1} \quad (37)$$

where $\beta' = \beta_{\text{eff}} - j \cdot \alpha_{\text{eff}}$, with β_{eff} and α_{eff} being the effective phase and attenuation constants, respectively, defined as

$$\beta_{\text{eff}} = \beta_1 - \text{Im}\left\{ \sum_{|i|>1} \frac{C_{1,i} \cdot a_i}{a_1} \right\} \quad (38)$$

$$\alpha_{\text{eff}} = -\text{Re}\left\{ \sum_{|i|>1} \frac{C_{1,i} \cdot a_i}{a_1} \right\}. \quad (39)$$

Therefore, we can consider that the parasitic couplings to cutoff modes cause a double effect in the expected behavior of the waveguide device obtained assuming single-mode operation: first, a continuous modification in the effective phase constant of the fundamental TE_{10} mode that is represented by the term of β_{eff}, and second, the term associated with α_{eff} describes the local "loss" or "recovery" of energy by the fundamental mode due to the coupling to cutoff modes that are able to locally store and "give back" the energy.

It is important to note that the effective complex propagation constant, $\beta' = \beta_{\text{eff}} - j \cdot \alpha_{\text{eff}}$, will no longer be constant in the propagation direction, z, since it depends on the complex amplitudes of the modes a_1 and a_i, as well as on the coupling coefficients of the form $C_{1,i}$, with $|i| > 1$, which are also variable with z. The average value of the effective complex propagation constant along the device, $\bar{\beta}'$, can be taken, to make the parameter constant with z again, as in the single-mode operation approach

$$\bar{\beta}' = \frac{\int_0^L (\beta_{\text{eff}} - j \cdot \alpha_{\text{eff}}) \cdot dz}{L} = \bar{\beta}_{\text{eff}} - j \cdot \bar{\alpha}_{\text{eff}} \quad (40)$$

where $\bar{\beta}_{\text{eff}}$ and $\bar{\alpha}_{\text{eff}}$ are the average effective phase and attenuation constants, respectively.

Now, it is important to realize that the effective attenuation term is locally not null, i.e., $\alpha_{\text{eff}}(z) \neq 0$. However, since the coupled-mode theory does not consider dissipative losses, the total power supplied to the rectangular waveguide structure in the fundamental mode must leave the structure also in that mode (all the higher order modes are under cutoff), and consequently, the average effective attenuation constant will satisfy $\bar{\alpha}_{\text{eff}} = 0$. Therefore, $\bar{\beta}'$ will be always real, verifying $\bar{\beta}' = \bar{\beta}_{\text{eff}}$. Employing the average value of the effective complex propagation constant, $\bar{\beta}' = \bar{\beta}_{\text{eff}}$, in (37), a coupled-mode equation that takes into account the effect of the cutoff modes with the only approximation of replacing β' by its average value $\bar{\beta}'$ is obtained

$$\frac{da_1}{dz} = -j \cdot \bar{\beta}_{\text{eff}} \cdot a_1 + C_{1,-1} \cdot a_{-1}. \quad (41)$$

As it can be seen, (41) is fully analogous to the coupled-mode equation of the single-mode operation assumption (32), just by considering the average effective phase constant, $\bar{\beta}_{\text{eff}}$, instead of the phase constant of the fundamental TE_{10} mode, β_1. Therefore, if we employ the single-mode operation assumption to synthetize a waveguide device, the expected frequency response will be shifted in frequency, because of the difference between the value used in the synthesis procedure, β_1, and the effective value resulting from the coupling to cutoff modes, $\bar{\beta}_{\text{eff}}$. Fortunately, the scaling property of the coupling coefficient reported in [41]

$$\psi \cdot K(z \cdot \psi) \leftrightarrow S_{11}\left(\frac{\beta}{\psi}\right) \quad (42)$$

can be applied to relate the required scaling of the propagation axis and coupling coefficient, with the shift produced in the frequency response in reflection. Thus, applying (42), the final propagation axis must be calculated as z/ψ, and the amplitude of the coupling coefficient must be scaled as $\psi \cdot K(z)$. The scaling factor, ψ, can be calculated as the quotient between the average effective phase constant, $\bar{\beta}_{\text{eff}}$, and the phase constant of the fundamental mode, β_1

$$\psi = \frac{\bar{\beta}_{\text{eff}}(f_t)}{\beta_1(f_t)} \quad (43)$$

being f_t the frequency where both phase constants, $\bar{\beta}_{\text{eff}}$ and β_1, are calculated. It must be noticed that the scaling factor, ψ, will also be slightly frequency-dependent. Therefore, the method proposed to take into account the effect of the reactive couplings to higher order cutoff modes when employing the single-mode coupled-mode equation system of (32) can be less accurate for frequencies far away from f_t. Taking f_t as the cutoff frequency of the filter is customarily a very good compromise.

B. Inverse Scattering Synthesis Method for Filters With High Rejection Level: Integral Layer Peeling

In order to synthesize a microwave filter with smooth profile and high rejection levels, we start from the simplified system of coupled-mode equations obtained in Section IV-A [see (32)]. As it has been explained, that simplified system is valid assuming single-mode operation or making an approximation to take into account the effect of the cutoff modes. Since the coupling coefficient, $K(z)$, is a real function in our formulation, (32) can be rewritten as a Zakharov–Shabat system of quantum mechanics obtaining [41], [46]

$$j \cdot \begin{bmatrix} \frac{d}{dz} & -K \\ K^* & \frac{-d}{dz} \end{bmatrix} \cdot \begin{bmatrix} a^+ \\ a^- \end{bmatrix} = \beta \cdot \begin{bmatrix} a^+ \\ a^- \end{bmatrix} \quad (44)$$

where $*$ stands for complex conjugate.

We introduce two linearly independent solutions of the Zakharov–Shabat system (two of the so-called Jost functions), which satisfy in the limit [46]

$$\lim_{z\to-\infty}\begin{bmatrix}\phi_1(z,\beta)\\ \phi_2(z,\beta)\end{bmatrix}=\begin{bmatrix}1\\0\end{bmatrix}\cdot e^{-j\cdot\beta\cdot z} \tag{45.a}$$

$$\lim_{z\to-\infty}\begin{bmatrix}\overline{\phi}_1(z,\beta)\\ \overline{\phi}_2(z,\beta)\end{bmatrix}=\begin{bmatrix}0\\1\end{bmatrix}\cdot e^{j\cdot\beta\cdot z}. \tag{45.b}$$

Now, in order to solve the synthesis problem, we assume that the coupling region (i.e., the designed filter) starts at $z=0$ and ends at $z=L$, and therefore, $K(z)=0$ for $z<0$ and $z>L$. A solution of the Zakharov–Shabat system (and of the coupled-mode equations) with the boundary conditions $a^+(z=0,\beta)=1$ and $a^-(z=L,\beta)=0$ (i.e., output port matched) can be obtained as a linear combination of the previous Jost functions (45) of the form [41], [44], [46]

$$\begin{bmatrix}u_1(z,\beta)\\ u_2(z,\beta)\end{bmatrix}=\begin{bmatrix}\phi_1(z,\beta)\\ \phi_2(z,\beta)\end{bmatrix}+S_{11}(\beta)\cdot\begin{bmatrix}\overline{\phi}_1(z,\beta)\\ \overline{\phi}_2(z,\beta)\end{bmatrix} \tag{46}$$

being

$$S_{11}(\beta)=\left.\frac{a^-(z=0,\beta)}{a^+(z=0,\beta)}\right|_{a^-(z=L,\beta)=0} \tag{47}$$

where the solution, $a^+(z,\beta)=u_1(z,\beta)$ and $a^-(z,\beta)=u_2(z,\beta)$, corresponds to the situation when the output port is matched, and the values at the input port of the filter are $a^+(z=0,\beta)=u_1(z=0,\beta)=1$ and $a^-(z=0,\beta)=u_2(z=0,\beta)=S_{11}(\beta)$.

Taking into account these considerations, and the behavior of the Jost functions at the limit (45) that will remain valid up to the input port of the filter at $z=0$ (since $K(z)=0$ for $z<0$), the validity of (46) can be easily verified.

One of the previous Jost functions (solution of the Zakharov–Shabat system) can be represented as [41], [46]

$$\begin{bmatrix}\phi_1(z,\beta)\\ \phi_2(z,\beta)\end{bmatrix}=\begin{bmatrix}1\\0\end{bmatrix}\cdot e^{-j\cdot\beta\cdot z}+\int_{-\infty}^{\infty}\begin{bmatrix}A_1(z,\tau)\\ A_2(z,\tau)\end{bmatrix}\cdot e^{-j\cdot\beta\cdot\tau}\cdot d\tau \tag{48}$$

where the first term corresponds to the propagation of the forward traveling wave in the absence of coupling region [behavior at the limit (45.a)], and $A_1(z,\tau)$ and $A_2(z,\tau)$ are the kernel functions that characterize the scattering effect produced by the coupling region (i.e., the designed filter).

Additionally, using symmetry properties of the Zakharov–Shabat system (44), it can be easily demonstrated that our two Jost functions are related as [46]

$$\begin{bmatrix}\overline{\phi}_1(z,\beta)\\ \overline{\phi}_2(z,\beta)\end{bmatrix}=\begin{bmatrix}\phi_2^*(z,\beta)\\ \phi_1^*(z,\beta)\end{bmatrix}. \tag{49}$$

It is important to note that β is the independent variable in the Zakharov–Shabat system, while frequency is the independent variable in the coupled-mode equations. Therefore, it is necessary to assume that variables β and frequency are univocally related in our device, and specifically, that β does not vary with z for a given frequency [41]. Actually, although the target filter specifications are usually given as a function of frequency, the variable β will be used in our formulation, making the resulting synthesis equations independent of the implementation technology.

Reformulating the problem in the time domain by applying an inverse Fourier transform to (46) [after having substituted (48) and (49)] and taking into account causality considerations, it can be demonstrated that the kernel functions $A_1(z,\tau)$ and $A_2(z,\tau)$ satisfy the so-called Gel'fand–Levitan–Marchenko (GLM) coupled integral equations [41], [44], [47]

$$\begin{aligned}&A_1(z,\tau)+\int_{-\infty}^{z}A_2^*(z,y)\cdot F(y+\tau)\cdot dy=0,\quad |z|>\tau\\ &A_2(z,\tau)+F(z+\tau)+\int_{-\infty}^{z}A_1^*(z,y)\cdot F(y+\tau)\cdot dy=0,\quad |z|>\tau\end{aligned} \tag{50}$$

where $F(\tau)$ is the inverse Fourier transform of the $S_{11}(\beta)$ parameter [see (16)], and the reformulation has been done, rigorously speaking, in the τ domain. It is interesting to note that the integration range in (50) has a lower limit of $-\infty$, different from the restricted lower limit taken in [41] and [47]. The reason is that the causality restriction $F(\tau)=0$ for $\tau<0$ is not applied in our case due to considerations explained later in this section.

Solving the GLM coupled integral equations (50), the kernel functions $A_1(z,\tau)$ and $A_2(z,\tau)$ can be calculated for a target frequency response, $S_{11}(\beta)$, expressed through $F(\tau)$ [see (16)]. An iterative solution to the GLM equations can be obtained, where the zero-order approximation is achieved by neglecting the integral terms as [41], [44], [47]

$$A_1(z,\tau)=0,\quad |z|>\tau \tag{51.a}$$

$$A_2(z,\tau)=-F(z+\tau),\quad |z|>\tau. \tag{51.b}$$

This zero-order approximation neglects the cases when multiple reflections occur at intermediate points of the filter structure. Only the cases with one scattering event are taken into account. This approximation is valid for filters with low reflectivity, or at the beginning (close to the input port) of general filters with high reflectivity. When multiple reflections within the structure (cases of multiple scattering events) cannot be neglected, higher order approximations of the iterative solution of the GLM equations can be employed [41], [44].

Additionally, due to causality considerations, it can be demonstrated that [41], [46]

$$A_1(z,\tau)=0,\quad z<|\tau| \tag{52.a}$$

$$A_2(z,\tau)=0,\quad z<|\tau|. \tag{52.b}$$

In order to solve the synthesis problem, we are going to divide the filter structure into several layers that will have a nonuniform profile. The iterative solution of the GLM equations will be employed to solve each of the layers. If the length of the layers is short enough, then the very simple zero-order approximation of (52) will be enough to solve the problem. Each of the layers will be solved consecutively, from the input to the output port of the filter. The synthesis method will be called integral layer peeling (ILP) and follows the same

principle as the technique proposed in [44] for reconstructing fiber Bragg gratings with high reflectivity in the optical field.

Recalling the solution previously obtained with the output port matched (46), and substituting (48) and (49), expressions for the forward traveling wave, $a^+(z,\beta)=u_1(z,\beta)$, and backward traveling wave, $a^-(z,\beta)=u_2(z,\beta)$, can be obtained as a function of $A_1(z,\tau)$ and $A_2(z,\tau)$ [44]. If the zero-order approximation of (51) is employed to calculate the kernel functions $A_1(z,\tau)$ and $A_2(z,\tau)$ in the range $z>\tau$ (fully included within the region of validity of the GLM equations), and the causality restrictions of (52) are applied to limit the integration range, then the forward and backward traveling waves will have the following expressions along the filter:

$$a^+(z,\beta)=e^{-j\cdot\beta\cdot z}-S_{11}(\beta)\cdot\int_{-\infty}^{z}F^*(z+\tau)\cdot e^{j\cdot\beta\cdot\tau}\cdot d\tau \tag{53.a}$$

$$a^-(z,\beta)=S_{11}(\beta)\cdot e^{j\cdot\beta\cdot z}-\int_{-\infty}^{z}F(z+\tau)\cdot e^{-j\cdot\beta\cdot\tau}\cdot d\tau \tag{53.b}$$

where the solution has been obtained with the boundary conditions $a^+(z=0,\beta)=1$ and $a^-(z=L,\beta)=0$ (i.e., output port matched), and is valid for low reflectivity, or in general at the beginning of the filter (the zero-order approximation of the iterative solution of the GLM equations has been employed). Now, the local reflection coefficient along the filter, $\rho(z,\beta)$, can be obtained from (53), after some mathematical manipulations, as

$$\rho(z,\beta)=\frac{a^-(z,\beta)}{a^+(z,\beta)}=e^{j\cdot2\cdot\beta\cdot z}\frac{S_{11}(\beta)-\bar{\rho}(\beta)}{1-S_{11}(\beta)\cdot\bar{\rho}^*(\beta)} \tag{54}$$

where

$$\bar{\rho}(\beta)=\int_{-\infty}^{2z}F(\tau)\cdot e^{-j\cdot\beta\cdot\tau}\cdot d\tau \tag{55}$$

and the expression achieved for $\rho(z,\beta)$ is valid for the same conditions as (53). In order to apply the ILP synthesis method, the filter will be divided into layers which have nonuniform profile and the same length, Δz. Since the coupled-mode equations are linear, the local reflection coefficient, $\rho(z,\beta)$, is identical to the reflection coefficient at the input of the filter section located at the region $[z,L]$. Thus, the reflection coefficient at the input of the mth layer (S_{11} parameter of the filter section located at $[m\cdot\Delta z,L]$) can be defined as

$$S_{11,m}(\beta)=\rho(m\cdot\Delta z,\beta) \tag{56}$$

and $S_{11,m}(\beta)$ can be propagated along the filter, through a layer of length Δz, by using (54) as

$$S_{11,m+1}(\beta)=e^{j\cdot2\cdot\beta\cdot\Delta z}\cdot\frac{S_{11,m}(\beta)-\bar{\rho}_m(\beta)}{1-S_{11,m}(\beta)\cdot\bar{\rho}_m^*(\beta)} \tag{57}$$

where

$$\bar{\rho}_m(\beta)=\int_{-\infty}^{2\cdot\Delta z}F_m(\tau)\cdot e^{-j\cdot\beta\cdot\tau}\cdot d\tau \tag{58}$$

and

$$F_m(\tau)=\frac{1}{2\pi}\int_{-\infty}^{\infty}S_{11,m}(\beta)\cdot e^{j\beta\tau}\cdot d\beta. \tag{59}$$

When the length of the layers, Δz, is short enough, (57) will be accurate since it is applied at the beginning of the corresponding filter section. If the use of longer layers is required, then higher order approximations of the iterative solution of the GLM equations could be employed to obtain (53), and from it (54) and (57).

Inspecting (58), it can be noted that since $F_m(\tau)$ is a causal function (it is the inverse Fourier transform of $S_{11,m}(\beta)$, i.e., the impulse response in reflection of the filter section at $[m\cdot\Delta z,L]$), the lower limit of the integral in (58) could be theoretically replaced by 0. However, in practice, $F_m(\tau)$ is numerically calculated from $S_{11,m}(\beta)$ using the inverse fast Fourier transform (iFFT), and due to the limited bandwidth and spectral resolution employed, $F_m(\tau)$ becomes slightly inaccurate and noncausal. The use of the lower integration limit of $-\infty$ in (58) significantly reduces the error caused by numerical inaccuracies, in the propagation of the reflection coefficient along the layers of the filter [44].

As it was demonstrated in [41], the coupling coefficient, $K(z)$, required to obtain a target frequency response, $S_{11}(\beta)$, can also be calculated through the kernel functions $A_1(z,\tau)$ and $A_2(z,\tau)$ of the GLM equations (50). Formulating the problem in the τ domain, by taking the inverse Fourier transform of the coupled-mode equations (32), substituting the solutions obtained (46), (48), (49), expressed also in the τ domain, and taking into account causality considerations (52), it can be deduced after several mathematical manipulations [41]

$$K(z)=-2\cdot F(2z)-2\int_{-z}^{z}A_1^*(z,y)\cdot F(y+z)\cdot dy \tag{60}$$

where $F(\tau)$ is the inverse Fourier transform of the target frequency response $S_{11}(\beta)$ [see (16)]. To obtain this expression, it has been assumed that $K(z)$ does not depend on β, or equivalently, on the frequency.

In order to calculate the coupling coefficient profile of a layer, (60) can be employed. If the length of the layer, Δz, is short enough, then the zero-order approximation (51) of the iterative solution of the GLM equations can be used, resulting in [41], [44]

$$K(z)=-2\cdot F(2z). \tag{61}$$

If the use of longer layers is required, then higher order approximations could be employed. An equation for $K(z)$ expressed as an infinite series solution, obtained from the iterative solution of the GLM equations, is given in [41].

Thus, the coupling coefficient required for the filter can be calculated layer by layer, where the contribution of the mth layer is (assuming that its length Δz is short enough) [44]

$$K(m\cdot\Delta z+z')=-2\cdot F_m(2z'),\quad 0\le z'\le\Delta z \tag{62}$$

with $F_m(\tau)$ given by (59).

Therefore, in order to synthesize a microwave filter with a target frequency response given by its $S_{11}(\beta)$ parameter,

we divide the filter structure into layers which have nonuniform profile and a length Δz short enough. We start from the input port of the filter placed at $z = 0$. That point corresponds to the input of the $m = 0$ layer. Then, we take $S_{11,m=0}(\beta) = S_{11}(\beta)$, and using (62), we calculate the coupling coefficient profile required for the $m = 0$ layer. Next, applying (57), we propagate $S_{11,m=0}(\beta)$ along the filter, obtaining $S_{11,m=1}(\beta)$ and effectively "peeling off" the $m = 0$ layer. Proceeding iteratively, calculating the coupling coefficient profile of the m layer with (62) and propagating $S_{11,m}(\beta)$ along the filter with (57), obtaining $S_{11,m+1}(\beta)$ and "peeling off" the m layer, we can continue until the end of the filter is reached at $z = L$. In this way, the coupling coefficient of the filter is calculated layer by layer, from the input to the output port.

It is interesting to note that in this synthesis method, the coupling coefficient profile calculated for each layer is not used to propagate the $S_{11,m}(\beta)$ parameter along the filter [see (57)]. Therefore, the error produced when calculating the filter profile does not accumulate along the filter through the layer peeling procedure [44]. This is an important advantage of the ILP method when compared to the continuous layer peeling (CLP) technique proposed in [43] and allows the new ILP method to synthesize filters with much higher rejection levels, without experiencing numerical problems.

V. Application: Synthesis of LPF in Rectangular Waveguide Oriented to Direct Metal AM

In this section, the feasibility of the novel design methodology thoroughly explained for the synthesis of smooth-profiled rectangular waveguide filters intended to be readily fabricated by means of direct metal AM techniques (i.e., growing the filter in the propagation direction without using auxiliary supports) will be demonstrated with a Ku-band WR75 LPF design example, where challenging satellite specifications will be required. The synthetized filter will be fabricated using SLM technology in AlSi10Mg aluminum alloy.

First, the required passband for the filter is defined from 10.7 to 11.7 GHz, with a return loss level larger than 20 dB for the whole band. Additionally, a minimum rejection level of 80 dB must be guaranteed for the stopband, located between 14 and 15 GHz. However, considering the typical $\pm$100-μm fabrication tolerances associated with SLM manufacturing in AlSi10Mg, it is advisable to include security margins in the target frequency response that will be finally synthetized, in order to ensure fulfillment of the initial specifications in the fabricated prototype. Applying this security margin criterion that is widely employed in practice, the passband of the filter will be from 10.6 to 11.75 GHz, with return loss level better that 25 dB, while the stopband with minimum rejection level of 80 dB must be achieved from 13.8 up to 15 GHz.

In order to synthetize a rectangular waveguide filter that will meet the aforementioned requirements in terms of frequency response and fabrication aspects, the first task is to select a starting commensurate-line UE prototype that satisfies the frequency specifications. It must be highlighted that this choice represents a critical design step since the smooth-profiled waveguide filter that will be finally synthetized using the ILP technique with an interpolated version of the impulse response of that initial UE prototype will feature similar physical dimensions (length and heights) to those of the initial UE prototype (see Figs. 1 and 2). Thus, the transitions between adjacent UEs exhibited by the initial commensurate-line UE prototype, and the length of the UEs, will provide an intuitive knowledge of the angles that will be eventually found in the synthetized smooth-profiled structure. Interestingly, the transitions of the starting UE prototype can be controlled by means of two filter design parameters: the filter order, N, and the frequency of maximum rejection, f_0 (or its corresponding phase constant, β_0) [see Fig. 6(b)]. If the filter order is increased while f_0 is decreased to keep the rejection level constant at a given frequency (80 dB at 13.8 GHz in our design example), the difference in characteristic impedance (or equivalently in height for rectangular waveguide technology) between any consecutive UEs will be reduced, and the resulting angle in the synthetized smooth-profiled filter will be smaller as a consequence. Additionally, when the value of f_0 is reduced, the length of the UEs (commensurate-line sections), l, is increased since it has an inverse proportional relationship with β_0 [see (19) and (22)]. Thus, the total length of the commensurate-line UE prototype is also increased, effectively stretching the profile of the synthesized smooth filter, diminishing the profile slope and its angles. It is worth noting that increasing the filter order makes the initial UE prototype also longer, so the synthetized smooth-profiled filter will be longer as well. Therefore, a tradeoff solution must be reached, keeping the filter profile angles small enough to be comfortably fabricated through direct metal AM (i.e., growing the filter in the propagation direction without using auxiliary supports) and having the filter length under control not to needlessly increase the passband insertion loss and the filter footprint.

Regarding the specific case of our design example, a Zolotarev LPF response was selected since it will provide less abrupt transitions between adjacent UEs compared to a Chebyshev response of the same order and cutoff frequency (while featuring a slightly more selective response) [35], which is desirable for an eventual SLM fabrication because of the reasons previously commented. A high filter order, $N = 21$, and a return loss level in the passband of 25 dB are taken to be able to fulfill the challenging frequency specifications. The frequency selected to exhibit the highest rejection level was $f_0 = 17.568$ GHz, which corresponds to a phase constant of $\beta_0 = 329.2$ rad/m, that can be calculated employing (27) and (28) for the case of the fundamental TE_{10} mode ($p_m = 1$ and $q_m = 0$) and the width of the WR75 standard, $a = 19.05$ mm. The upper value of the passband (including security margin) was taken as the cutoff frequency of the filter, i.e., $f_c = 11.75$ GHz, leading to a cutoff phase constant of $\beta_c = 182.89$ rad/m. Furthermore, the value selected for the minimum frequency of the passband was $f_{Zolo} = 8.298$ GHz, yielding to an associated phase constant $\beta_{Zolo} = 55.20$ rad/m. Since β_0, β_c, and β_{Zolo} are known, and taking into account that all the commensurate-line sections of the UE prototype have identical electrical length at β_0 of $\theta_0 = \pi/2$ rad, the electrical length of the line sections for β_c and β_{Zolo} can also be determined by (5), being $\theta_c = 0.873$ rad and $\theta_{Zolo} = 0.263$ rad.

TABLE I
PROTOTYPE UE VALUES

Unit Element	Zolotarev heights (mm)	Modified heights (mm)
b_S=b_L	9.525	9.525
b_1=b_{21}	5.914	5.510
b_2=b_{20}	10.838	9.284
b_3=b_{19}	2.933	2.446
b_4=b_{18}	7.946	7.646
b_5=b_{17}	1.412	2.057
b_6=b_{16}	4.100	9.185
b_7=b_{15}	0.646	2.253
b_8=b_{14}	1.989	9.525
b_9=b_{13}	0.337	2.153
b_{10}=b_{12}	1.217	8.882
b_{11}	0.259	1.984

Finally, the frequency parameters of the 21st order all-pole normalized Zolotarev response can be calculated by means of (8), i.e., the normalized cutoff frequency has the expected value of $\omega_c = 1$ rad/s and the normalized minimum frequency of the passband is $\omega_{\text{Zolo}} = 0.34$ rad/s, while the normalized frequency that specifies the highest rejection level that will be achieved with the commensurate-line UE prototype is $\omega = \alpha = 1/\sin\theta_c = 1.305$ rad/s (see Fig. 3). Once the normalized frequency values ω_c, ω_{Zolo}, and α, have been defined, and the filter order N and return loss in the passband have also been selected, the normalized all-pole low-pass Zolotarev response is completely determined [35]. Then, using (9), the normalized response can be translated to the Richards' transform domain (see Section II). Finally, the values of the UEs (characteristic impedances or equivalently heights for rectangular waveguide technology [35]) of the commensurate-line UE prototype that satisfies the intended frequency response can be calculated in the Richards' transform domain, as explained in Section II. The results are given in Table I. As it can be seen, the height of the input port, b_S, and of the output port, b_L, is fixed to the value of the WR75 standard, $b_S = b_L = 9.525$ mm. This is done for convenience since if all the UE values are multiplied by a constant, the frequency response of the prototype remains unaltered [35].

It must be highlighted that the minimum height of the commensurate-line UE prototype of the Zolotarev filter is $b_{11} = 0.259$ mm, which is a value that may become troublesome for the SLM manufacturing tolerances (± 100 μm). Since the final smooth-profiled filter that will be synthetized from an interpolated version of the impulse response of this commensurate-line UE prototype will retain a similar length and height excursion, it will be advisable to find more suitable dimensions for the initial commensurate-line UE prototype. For doing so, an optimization procedure was performed using Keysight Genesys by requiring a minimum UE value (height in our case of rectangular waveguide) of 1.75 mm and a maximum UE value (height) of 9.525 mm for the commensurate-line prototype, while still demanding the fulfillment of the frequency response requirements. This quick optimization procedure gave rise to a modified Zolotarev commensurate-line UE prototype, and its UE values are also given in Table I. A comparison between the frequency responses of the canonical and modified Zolotarev UE prototypes is shown in Fig. 7, where the masks required for the return loss and rejection levels are also included for the sake of completeness.

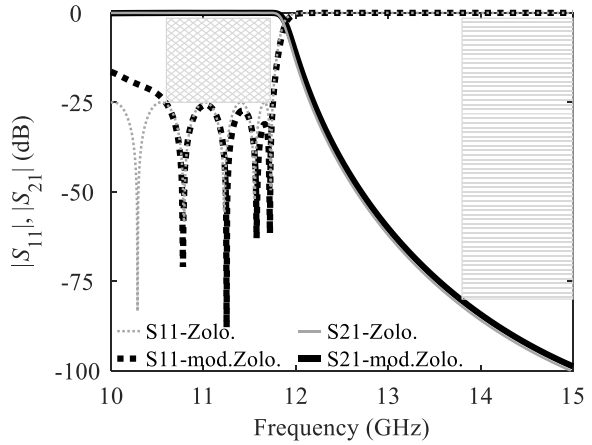

Fig. 7. Comparison between the frequency responses, $|S_{11}|$ and $|S_{21}|$, of the Zolotarev and the modified-Zolotarev commensurate-line UE prototypes. The specifications required (including security margins) for the return loss (rhombus-based pattern mask) and for the rejection level (rectangle-based pattern mask) are also included.

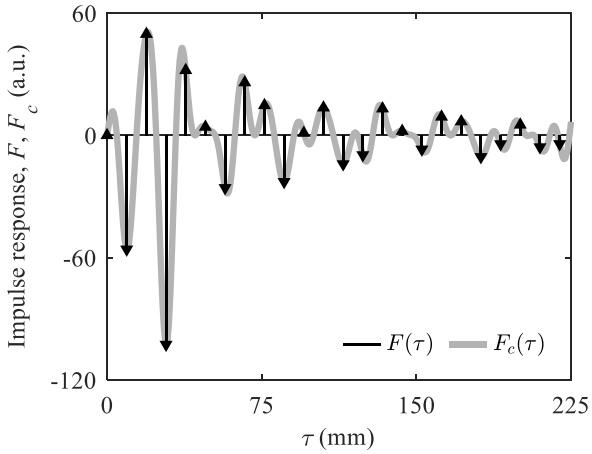

Fig. 8. Impulse response in reflection of the modified-Zolotarev commensurate-line UE prototype, $F(\tau)$, and underlying continuous impulse response, $F_c(\tau)$, obtained by performing a bandlimited interpolation with $m = 2$.

Once a valid commensurate-line UE prototype was found, its impulse response in reflection, $F(\tau)$, was calculated by means of the procedure explained in the Appendix, obtaining the values for the a_n coefficients (see Fig. 8). Then, the bandlimited interpolation of (20) was applied to obtain the underlying continuous impulse response in reflection, $F_c(\tau)$, that will be eventually employed as target response in the synthesis process. As it is explained in Section III, $m = 2$ must be selected in (21) to achieve an LPF response and thus, $\beta_{\max} = 2 \cdot \beta_0$ will be employed. A numerical discretization period in τ of value $T_\tau/40$ [where T_τ can be obtained from (22)] was employed for an impulse response $F_c(\tau)$ defined between $\tau = 0$ and $\tau = 8000 \cdot T_\tau$. The corresponding frequency response in reflection, $S_{11,c}(\beta)$, was defined accordingly from $\beta = 0$ up to $\beta = 40 \cdot \beta_0$, with a discretization period in β of value $\beta_0/2000$. In order to efficiently calculate the bandlimited interpolation of (20), the MATLAB "interpft.m" function can be employed in practice with a much lower numerical cost. The obtained $F_c(\tau)$ is shown in Fig. 8. However, it must be

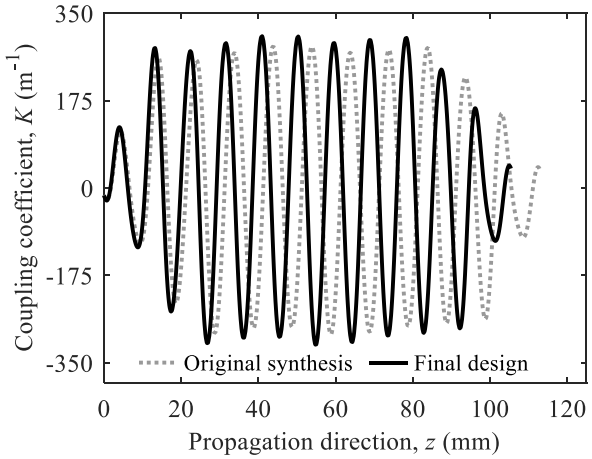

Fig. 9. Coupling coefficient, K, along the propagation axis, z, calculated using the ILP synthesis technique for the interpolated impulse response in reflection of the modified-Zolotarev UE prototype, $F_c(\tau)$: original synthesis, and final coupling coefficient obtained after the compensation of the effect of the cutoff modes.

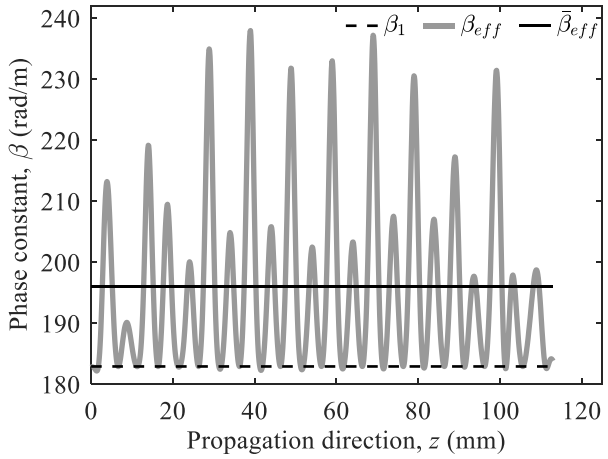

Fig. 11. Phase constant of the fundamental TE_{10} mode at the compensation frequency, $f_t = 11.75$ GHz, β_1, effective phase constant caused by cutoff modes, β_{eff}, along the propagation direction, z, for the same frequency, and its average value, $\bar{\beta}_{\text{eff}}$.

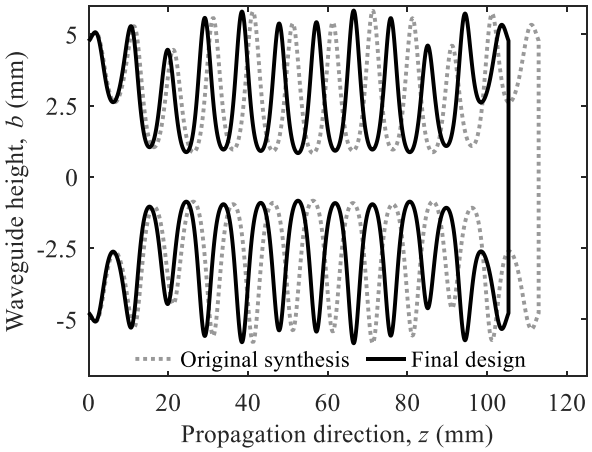

Fig. 10. Waveguide height profile, $b(z)$, associated with both versions of the coupling coefficient, $K(z)$: original synthesis and final design obtained after the compensation of the effect of the cutoff modes.

pointed out that $m-1$ samples with zero value must be inserted between each pair of samples of $F(\tau)$, prior to employing the function "interpft.m" to compute (20). By doing so, it will be ensured that $\beta_{\max} = m \cdot \beta_0$ as stated in (21).

Once the target interpolated impulse response in reflection, $F_c(\tau)$, was determined, the ILP synthesis technique carefully explained in Section IV-B was applied, using a layer thickness of $\Delta z = 3 \cdot T_\tau/80$ (i.e., three times the numerical discretization period selected for the propagation axis), to calculate the required coupling coefficient, $K(z)$. The fast Fourier transform (FFT) algorithm was employed to efficiently compute the integral of (58). The coupling coefficient obtained is shown in Fig. 9, in gray dotted line. The length of the synthetized structure is $L = 113$ mm.

After having determined $K(z)$, the rectangular waveguide height profile along the propagation direction, $b(z)$, can be immediately calculated by applying (34) with an input port height set to the WR75 standard, i.e., $b(0) = 9.525$ mm. The attained height profile is depicted in Fig. 10, in gray dotted line. The minimum height of the synthetized waveguide structure is 1.67 mm, being large enough to be safely fabricated with the SLM technique. Furthermore, the maximum height obtained along the synthesized waveguide is $\max\{b(z)\} = 11.67$ mm. The cutoff frequency of the first relevant higher order modes (TE_{12} and TM_{12}) that can get coupled to the fundamental TE_{10} mode in our rectangular waveguide device with symmetrical variations in height is calculated for $\max\{b(z)\}$, resulting in 26.87 GHz. Therefore, the maximum height guarantees that all the relevant higher order modes are kept in cutoff regime throughout the whole filter structure, for all the operation bandwidth of the filter. This is the main requirement of the method proposed in Section IV-A2 for the compensation of the parasitic effects of the cutoff modes.

In order to determine the scaling factor, ψ, which is needed to compensate for the reactive coupling to cutoff modes, the first step is to analyze the synthetized waveguide structure using the coupled-mode equation system of (26) for a frequency, f_t. The value selected for this compensation frequency was $f_t = f_c = 11.75$ GHz, so as to adjust the cutoff frequency of the filter, f_c, with the best accuracy. As it has been previously calculated, the phase constant of the fundamental TE_{10} mode at $f_t = 11.75$ GHz is $\beta_1(f_t = 11.75\text{GHz}) = 182.89$ rad/m. The coupling coefficients, $C_{m,\pm i}^{\text{TE-TE}}$, $C_{m,\pm i}^{\text{TE-TM}}$, and $C_{m,\pm i}^{\text{TM-TM}}$, between all the relevant modes that must be considered for our case of a nonuniform rectangular waveguide with symmetrical variations in height, excited with the fundamental TE_{10} mode (see Section IV-A), were calculated employing (31.a)–(31.c), respectively. Once all the necessary coupling coefficients were determined, the coupled-mode equation system of (26) was numerically solved using the MATLAB "bvp4c.m" function, with the proper boundary conditions previously explained in Section IV-A. Due to the fact that a finite number of modes must be selected in order to numerically solve (26), a maximum modal index $q = 128$ was chosen for both TE and TM modes, ensuring very high convergence for the complex amplitudes of the modes obtained, $a_i(z)$. The effective phase constant, β_{eff}, was calculated by means of (38) from the $C_{m,\pm i}^{\text{TE-TE}}$, $C_{m,\pm i}^{\text{TE-TM}}$, $C_{m,\pm i}^{\text{TM-TM}}$, and $a_i(z)$ previously obtained, and the result is given in Fig. 11, together with the phase constant of the

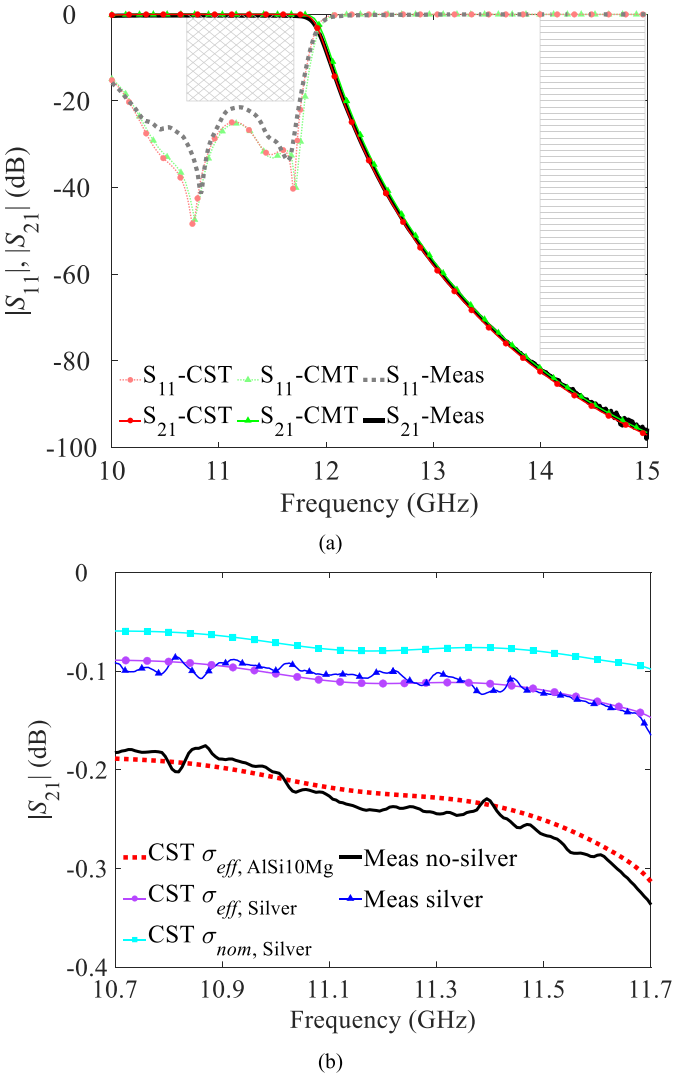

Fig. 12. (a) CST MWS simulated, coupled-mode theory simulated, and measured $|S_{11}|$ and $|S_{21}|$ parameters of the final modified-Zolotarev LPF, fabricated in AlSi10Mg using an SLM machine. The specifications required for the return loss (rhombus-based pattern mask) and for the rejection level (rectangle-based pattern mask) are also included. (b) Detail of $|S_{21}|$ parameter in the passband, without silver plating and after silver plating, where the effective conductivity deduced for AlSi10Mg ($\sigma_{\text{eff,AlSi10Mg}} = 6.2 \cdot 10^6$ S/m), the effective conductivity deduced for silver ($\sigma_{\text{eff,Silver}} = 2.8 \cdot 10^7$ S/m), and the nominal conductivity of silver ($\sigma_{\text{nom,Silver}} = 6.3 \cdot 10^7$ S/m) are taken in the CST MWS simulations.

fundamental TE_{10} mode. The average effective phase constant, $\bar{\beta}_{\text{eff}} = 196.65$ rad/m, was determined using (40), and it is also depicted in Fig. 11. Finally, the value of the scaling factor at the compensation frequency $f_t = f_c = 11.75$ GHz, $\psi = 1.075$, was obtained by means of (43). The scaling factor was applied to $K(z)$ according to (42), and the resulting final coupling coefficient is depicted in Fig. 9, in black solid line. The final height profile for the rectangular waveguide filter was calculated by means of (34), taking again $b(0) = 9.525$ mm (WR75 standard port), and the results are given in Fig. 10, in black solid line. The final synthetized waveguide filter was simulated with CST Microwave Studio (MWS) (assuming perfect conductor) and solving the coupled-mode equations (maximum modal index $q = 16$). The results, shown in Fig. 12(a), confirm the accuracy of the coupled-mode theory employed and the fulfillment of all the required specifications, as it can be seen from their corresponding masks also included in Fig. 12(a). The final length of the filter is $L = 105$ mm.

The resulting modified-Zolotarev filter was fabricated in a single piece, by means of a direct metal AM technique known as SLM, employing a Renishaw RenAM 500M system and using AlSi10Mg alloy as the material for the powder. The filter was grown following its propagation direction, i.e., aligning the filter propagation axis, z, with the building chamber vertical direction. As it was explained in Section I, this choice of growing direction has clear advantages. The first one is that additional supporting structures were not needed since the filter does not feature neither overhanging walls nor critical angles, and consequently, we can consider the smooth-profiled synthetized filter as a self-supporting structure in that direction. It is worth noting that in most of the cases, like in our design example, the device obtained following the design procedure will satisfy the self-supporting condition immediately. However, if the angles formed between the filter profile and its transversal plane are not high enough, then the filter height $b(z)$ can be multiplied by a constant minor than one, keeping the coupling coefficient $K(z)$ unaltered [see (33)], but diminishing the profile slope and increasing the angle with respect to the transversal plane of the filter. In this case, proper tapers should be added at the input and output ports of the filter to keep the standard port dimensions, as it was done in [42]. The taper design procedure is thoroughly explained in [48]. Another important advantage of growing the filter following its propagation axis is that the classical staircase effects experienced in SLM fabrications are reduced and optimum manufacturing accuracy is achieved, as it was discussed in Section I.

Once the filter was fabricated, a mechanical postprocessing procedure that consisted in polishing both flanges was performed, looking for an improvement of their flatness as well as a significant reduction of their roughness, since the surface finish quality of these zones may become critical in the subsequent characterization stage.

At this point, the filter was measured with an Agilent E8364B PNA vector network analyzer, employing WR75 coaxial-to-waveguide transitions and their calibration kit. The obtained results are depicted in Fig. 12(a). A very good agreement between the simulation and measurement results can be observed, and the frequency specifications required for the filter are fully satisfied. The slight differences found between the simulations and measurements can be attributed to the SLM fabrication tolerances and to the losses of the AlSi10Mg alloy. In order to minimize the insertion loss, an additional postprocessing step was applied to a second prototype (with identical nominal dimensions) by performing a silver coating of thickness 10 μm over the whole surface of the structure. The silver plating was performed using a standard electrolytic process (commonly referred to in the literature as electrolytic plating or electroplating), widely employed for standard waveguide filters. The direct path existent between the input and output ports of the filter and the smooth profile make this process feasible and very convenient for our device, even in its single-piece format [22]. A photograph

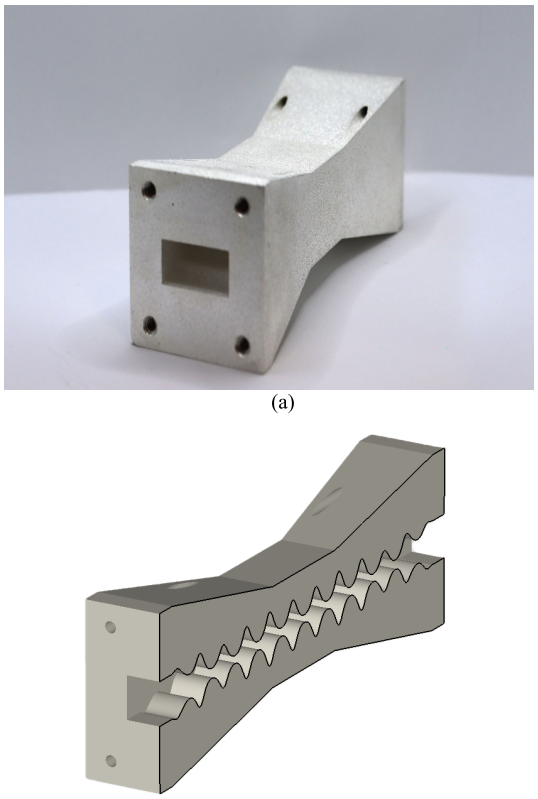

(a)

(b)

Fig. 13. (a) Photograph and (b) schematic inner view of the final Ku-band modified-Zolotarev LPF fabricated through direct metal AM (Renishaw RenAM 500M SLM machine).

of the final filter, together with a schematic inner view, is provided in Fig. 13. The filter was measured again after the silver plating process, employing the same measurement setup as in the first characterization. The result is shown in Fig. 12(b), together with the measurement obtained prior to silver plating (AlSi10Mg). The corresponding CST MWS simulations are also included, using the nominal conductivity of silver ($\sigma = 6.3 \cdot 10^7$ S/m) and an effective conductivity (including the effect of surface roughness) for silver of $\sigma = 2.8 \cdot 10^7$ S/m (effective resistivity of 3.6 $\mu\Omega \cdot$ cm) and for AlSi10Mg of $\sigma = 6.2 \cdot 10^6$ S/m (effective resistivity of 16 $\mu\Omega \cdot$ cm), deduced from the measurements and in line with the values reported for microwave filters fabricated in AlSi10Mg through SLM, with and without silver plating, respectively [6], [12], [13], [15], [16], [18]. As it was expected, a reduction of the insertion loss is achieved and a final worst value for the measured insertion loss of 0.16 dB is obtained at the upper limit of the passband.

Finally, in order to check the out-of-band behavior of the filter, it was simulated (CST MWS and coupled-mode theory) and measured (Agilent E8364B PNA) in a much wider frequency range (up to 25 GHz), far beyond the standard operation range of the WR75 ports (10–15 GHz). To carry out the measurements above 15 GHz, proper coaxial-to-waveguide transitions (WR62 and WR42) and tapers to connect them to the WR75 filter ports were employed, ensuring excitation with the fundamental TE_{10} mode as intended. The results are given in Fig. 14, showing a very good agreement between

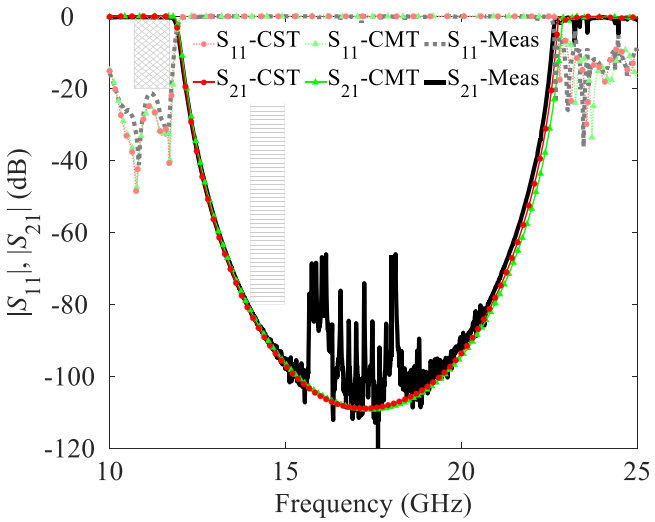

Fig. 14. CST MWS simulated, coupled-mode theory simulated, and measured $|S_{11}|$ and $|S_{21}|$ parameters of the final modified-Zolotarev LPF, fabricated in AlSi10Mg using an SLM machine. The out-of-band behavior of the filter is shown. The specifications required for the return loss (rhombus-based pattern mask) and for the rejection level (rectangle-based pattern mask) are also included.

the simulated and measured data. The spikes present in the measured rejected band (always below −60 dB) are due to the spurious excitation of the TE_{20} mode (cutoff frequency $f_{c,TE_{20}} = 15.74$ GHz), which could also be rejected if required by smoothly modulating the filter width as explained in [49].

As it can be seen, the obtained simulation and measurement results confirm the very good performance of the design technique proposed in this article for the synthesis of rectangular waveguide filters oriented to be easily fabricated with direct metal AM techniques.

VI. Conclusion

A novel design methodology for rectangular waveguide filters with smooth profile suitable for direct metal AM has been proposed and successfully demonstrated. The design technique can implement any all-pole transfer function, starting from a commensurate-line distributed UE prototype and interpolating its impulse response to obtain the target response for the smooth-profiled filter. Then, a novel inverse scattering synthesis technique is applied to synthesize the rectangular waveguide filter, relying on the coupled-mode theory to model the electromagnetic behavior of the waveguide. The new inverse scattering technique, known as ILP, allows us to synthesize filters with very high rejection levels, as customarily required in rectangular waveguide, without experiencing numerical problems. Although the methodology has been formulated for rectangular waveguide with variations in height, it could also be extended to variations in width by applying the technique developed in [48], and even to other waveguide technologies.

The design method has been demonstrated with a Ku-band rectangular waveguide LPF, fulfilling stringent satellite specifications, and fabricated through SLM. The prototype has been grown aligning the filter propagation axis in the vertical building direction, avoiding the need of supports, and achieving an optimum configuration for SLM fabrication. A very good agreement is obtained between the simulated and

measured results, confirming the accuracy and reliability of the proposed design method for filters intended for direct metal AM fabrication. Even though an LPF has been designed as example, the method could also be applied to bandpass filters as explained in this article.

As it can be seen in the design example and is reported in other articles [6], [13], [16], [18], using AlSi10Mg alloy to fabricate microwave filters through SLM, an effective conductivity that is adequate for many applications is achieved. Thus, silver plating of the inner surfaces of the filters can be avoided for many applications, easing and speeding the fabrication process.

The typical fabrication tolerances associated with SLM make this process suitable for microwave filters working below 20–30 GHz [6]. However, other direct metal AM technique with increased accuracy, resolution, and surface quality, known as microlaser sintering or micro-SLM, has been recently proposed for filters operating at higher frequencies. The technique was successfully employed to fabricate a W-band rectangular waveguide bandpass filter, with central frequency of 90 GHz, demonstrating its applicability to filters working at those higher frequencies [6], [50].

APPENDIX

The impulse response in reflection of the commensurate-line UE prototype of Figs. 1 and 2 can be readily calculated from the values of the characteristic impedances, Z_i, of the prototype. The impulse response will be formed by a sequence of equidistant impulses with coefficients a_n, whose values are identical in the time and τ domains [see (10) and (18)]. The coefficients a_n can be calculated following the method detailed below.

The procedure is based on the fact that a wave injected at the input port of the commensurate-line UE prototype will be scattered by each discontinuity encountered while propagating throughout the structure. As it is shown in Figs. 1 and 2, the prototype can be represented as a cascade of N commensurate lines, or UEs, all with the same electrical length, $\theta = \beta l$, but with different characteristic impedances, Z_i, plus an additional input and output line sections with the port impedances, named as $Z_0 = Z_S$ and $Z_{N+1} = Z_L$ for our calculations (see Fig. 15). At the junction between two commensurate lines with different characteristic impedances Z_{j-1} and Z_j, a discontinuity will arise, giving rise to a reflection and a transmission coefficient for the impinging wave with values [40]

$$\Gamma_{j-1,j} = \frac{Z_j - Z_{j-1}}{Z_j + Z_{j-1}} \tag{A1}$$

$$T_{j-1,j} = 1 + \Gamma_{j-1,j} = \frac{2 \cdot Z_j}{Z_j + Z_{j-1}}. \tag{A2}$$

Thus, wave propagation along the analyzed prototype can be described in terms of an infinite sum of the transmitted and reflected waves at each junction between two consecutive commensurate lines, taking into account the multiple reflection and transmission events arising throughout the structure.

If the incident wave at the input port of the prototype is a unit impulse, then the impulse response will be obtained. We are interested in calculating the impulse response in reflection, in the time or τ domain. For doing so, we need to calculate the coefficients of the impulse train, a_n [see (10) and (18)]. In order to determine them, we are going to define a time index, i, with time $t = i \cdot l/v_p$ for ideal transmission line, and $\tau = i \cdot l$ for the more general case of β constant with position. Additionally, the number of commensurate line will be represented by the j index, including the input and output port lines, numbered 0 and $N+1$, respectively (see Fig. 15). The forward traveling impulses are tracked just at the end of the commensurate lines and are represented at the F columns. The backward traveling impulses are tracked just at the beginning of the commensurate lines and are represented at the B columns. The straight and dashed arrows represent the transmission and reflection events, respectively. The circles, on the other hand, represent each contribution to the tracked impulses (see Fig. 15). It is interesting to note that a forward traveling impulse, when reflected, produces a new backward traveling impulse, and when transmitted a new forward traveling impulse. Conversely, a backward traveling impulse, when reflected, produces a new forward traveling impulse, and when transmitted a new backward traveling impulse. These reflection and transmission calculations will be the core of the algorithm employed to obtain the impulse response in reflection of the prototype. The algorithm is described now in detail.

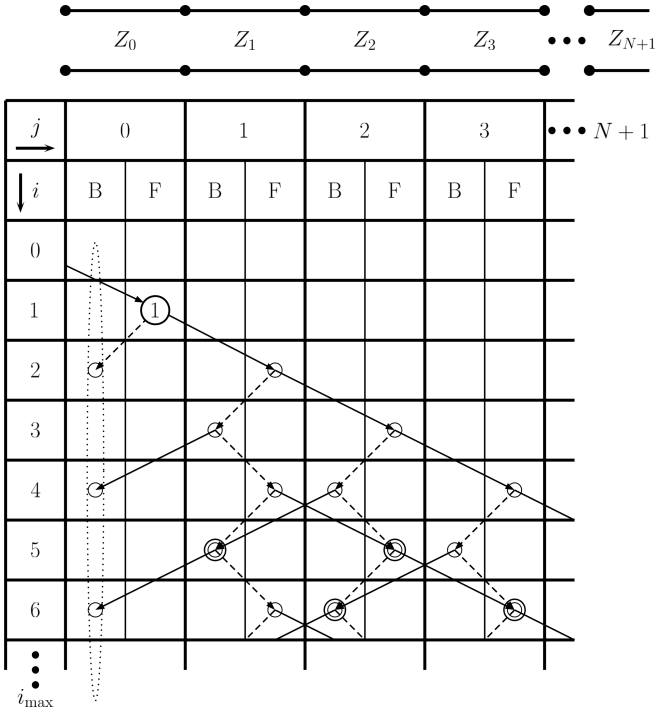

Fig. 15. Schematic representation for the algorithm to calculate the impulse response in reflection of the commensurate-line UE prototype shown above. A time index, i, with time $t = i \cdot l/v_p$ or $\tau = i \cdot l$, and a position index, j, where j is the number of commensurate line (including the input and output port lines, 0 and $N+1$), are employed. The forward and backward traveling impulses are tracked just at the end and beginning of the commensurate lines, respectively, and are represented at the corresponding F and B columns. To obtain the impulse response, the prototype is excited with a unit impulse injected at the input port, $F(i=1, j=0) = 1$. Straight and dashed arrows represent the transmission and reflection events, respectively, while the circles represent each contribution to the tracked impulses. The sought impulse response in reflection is formed by a sequence of equidistant impulses, separated $T = 2 \cdot l/v_p$ or $T_\tau = 2 \cdot l$ apart, with coefficients a_n, encircled by a dotted line at the input port line $a_n = B(i = 2 \cdot n, j = 0)$.

Step 1: Initialize the coefficients of the forward and backward traveling impulses tracked in the calculations, assuming excitation by a unit impulse at the input port.

//for all the considered time instants

$$\forall i = 0, 1, \ldots, i_{\max}$$

//for all the commensurate lines

$$\forall j = 0, 1, \ldots, (N+1)$$

//coefficients of forward traveling impulses

$$F(i, j) = 0$$

//coefficients of backward traveling impulses

$$B(i, j) = 0$$

//unit impulse injected at the input port

$$F(i = 1, j = 0) = 1.$$

Step 2: Propagation and scattering (reflection and transmission) of the impulses, through the commensurate-line prototype and the time or τ domain.

//for all the considered time instants
For $i = 1, 2, \ldots, (i_{\max} - 1)$
{
//for all the commensurate lines
For $j = 0, 1, \ldots, N$
{
//contributions of the forward traveling impulse,
//with coefficient $F(i, j)$, located at the i time instant
//at the end of the j commensurate line,
//for the next $i + 1$ time instant

$$F(i+1, j+1) = F(i+1, j+1) + F(i, j) \cdot T_{j,j+1}$$
$$B(i+1, j) = B(i+1, j) + F(i, j) \cdot \Gamma_{j,j+1}$$

//contributions of the backward traveling impulse,
//with coefficient $B(i, j)$, located at the i time instant
//at the beginning of the j commensurate line,
//for the next $i + 1$ time instant
If $j \neq 0$

$$\{F(i+1, j) = F(i+1, j) + B(i, j) \cdot \Gamma_{j,j-1}$$
$$B(i+1, j-1) = B(i+1, j-1) + B(i, j) \cdot \mathrm{T}_{j,j-1}\}$$

}
}.

Step 3: Extract the impulse response in reflection of the analyzed prototype, formed by a sequence of equidistant impulses, separated $T = 2 \cdot l/v_{\mathrm{p}}$ or $T_\tau = 2 \cdot l$ apart, with coefficients a_n [see (10) and (18)], by recovering the values of the a_n coefficients.

//coefficients of the backward traveling impulses
//at the input line ($j = 0$), and at the even time instants,
//since in the algorithm $t = i \cdot l/v_{\mathrm{p}}$ or $\tau = i \cdot l$

$$a_n = B(i = 2 \cdot n, j = 0).$$

REFERENCES

[1] J. P. Kruth, M. C. Leu, and T. Nakagawa, "Progress in additive manufacturing and rapid prototyping," *CIRP Ann.-Manuf. Technol.*, vol. 47, no. 2, pp. 525–540, 1998.

[2] A. Vafadar, F. Guzzomi, A. Rassau, and K. Hayward, "Advances in metal additive manufacturing: A review of common processes, industrial applications, and current challenges," *Appl. Sci.*, vol. 11, no. 3, p. 1213, Jan. 2021.

[3] R. Sorrentino and O. A. Peverini, "Additive manufacturing: A key enabling technology for next-generation microwave and millimeter-wave systems," *Proc. IEEE*, vol. 104, no. 7, pp. 1362–1366, Jul. 2016.

[4] J. M. Jafferson, H. Vinu, and K. Sekaran, "A study of additive manufacturing technologies and metallizing techniques for microwave waveguide components," *Mater. Today, Proc.*, vol. 46, pp. 1328–1334, Jan. 2021.

[5] F. Calignano et al., "Overview on additive manufacturing technologies," *Proc. IEEE*, vol. 105, no. 4, pp. 593–612, Apr. 2017.

[6] C. Tomassoni, O. A. Peverini, G. Venanzoni, G. Addamo, F. Paonessa, and G. Virone, "3D printing of microwave and millimeter-wave filters: Additive manufacturing technologies applied in the development of high-performance filters with novel topologies," *IEEE Microw. Mag.*, vol. 21, no. 6, pp. 24–45, Jun. 2020.

[7] J. A. Lorente, M. M. Mendoza, A. Z. Petersson, L. Pambaguian, A. A. Melcon, and C. Ernst, "Single part microwave filters made from selective laser melting," in *Proc. Eur. Microw. Conf. (EuMC)*, Sep. 2009, pp. 1421–1424.

[8] B. Zhang and H. Zirath, "3D printed iris bandpass filters for millimetre-wave applications," *Electron. Lett.*, vol. 51, no. 22, pp. 1791–1793, Oct. 2015.

[9] O. A. Peverini et al., "Enhanced topology of E-plane resonators for high-power satellite applications," *IEEE Trans. Microw. Theory Techn.*, vol. 63, no. 10, pp. 3361–3373, Oct. 2015.

[10] V. T. di Crestvolant, P. M. Iglesias, and M. J. Lancaster, "Advanced Butler matrices with integrated bandpass filter functions," *IEEE Trans. Microw. Theory Techn.*, vol. 63, no. 10, pp. 3433–3444, Oct. 2015.

[11] P. Booth, J. Gilmore, E. V. Lluch, and M. Harvey, "Enhancements to satellite feed chain performance, testing and lead-times using additive manufacturing," in *Proc. 10th Eur. Conf. Antennas Propag. (EuCAP)*, Apr. 2016, pp. 1–5.

[12] P. Booth and E. V. Lluch, "Enhancing the performance of waveguide filters using additive manufacturing," *Proc. IEEE*, vol. 105, no. 4, pp. 613–619, Apr. 2017.

[13] O. A. Peverini et al., "Integration of an H-plane bend, a twist, and a filter in Ku/K-band through additive manufacturing," *IEEE Trans. Microw. Theory Techn.*, vol. 66, no. 5, pp. 2210–2219, May 2018.

[14] P. Martin-Iglesias and B. Bonvoisin, "The potential of Additive Manufacturing for RF/microwave hardware: ESA perspective," in *Proc. Microw. Technol. Techn. Workshop*, Noordwijk, The Netherlands, Apr. 2017, pp. 1–32.

[15] O. A. Peverini et al., "Additive manufacturing of Ku/K-band waveguide filters: A comparative analysis among selective-laser melting and stereo-lithography," *IET Microw., Antennas Propag.*, vol. 11, no. 14, pp. 1936–1942, Nov. 2017.

[16] O. A. Peverini et al., "Selective laser melting manufacturing of microwave waveguide devices," *Proc. IEEE*, vol. 105, no. 4, pp. 620–631, Apr. 2017.

[17] F. Calignano, D. Manfredi, E. P. Ambrosio, L. Iuliano, and P. Fino, "Influence of process parameters on surface roughness of aluminum parts produced by DMLS," *Int. J. Adv. Manuf. Technol.*, vol. 67, nos. 9–12, pp. 2743–2751, 2013.

[18] R. G. Edwards, C. M. Norton, J. E. Campbell, and D. Schurig, "Effective conductivity of additive-manufactured metals for microwave feed components," *IEEE Access*, vol. 9, pp. 59979–59986, 2021.

[19] F. Calignano, "Design optimization of supports for overhanging structures in aluminum and titanium alloys by selective laser melting," *Mater. Des.*, vol. 64, pp. 203–213, Dec. 2014.

[20] P. Das, R. Chandran, R. Samant, and S. Anand, "Optimum part build orientation in additive manufacturing for minimizing part errors and support structures," *Proc. Manuf.*, vol. 1, pp. 343–354, Jan. 2015.

[21] R. V. Snyder, G. Macchiarella, S. Bastioli, and C. Tomassoni, "Emerging trends in techniques and technology as applied to filter design," *IEEE J. Microw.*, vol. 1, no. 1, pp. 317–344, Jan. 2021.

[22] P. A. Booth and E. V. Lluch, "Realising advanced waveguide bandpass filters using additive manufacturing," *IET Microw., Antennas Propag.*, vol. 11, no. 14, pp. 1943–1948, Nov. 2017.

[23] P. Booth, "Additive manufactured bandpass filters at Ka-band," in *IEEE MTT-S Int. Microw. Symp. Dig.*, Jul. 2019, pp. 7–9.

[24] S. W. Sattler, F. Gentili, R. Teschl, and W. Bosch, "Direct metal printed 4th order stepped impedance filter in the C/X band," in *IEEE MTT-S Int. Microw. Symp. Dig.*, Jun. 2018, pp. 145–148.

[25] F. Calignano et al., "Investigation of accuracy and dimensional limits of part produced in aluminum alloy by selective laser melting," *Int. J. Adv. Manuf. Technol.*, vol. 88, nos. 1–4, pp. 451–458, Jan. 2017.

[26] P. I. Richards, "Resistor-transmission-line circuits," *Proc. IRE*, vol. 36, no. 2, pp. 217–220, Feb. 1948.

[27] H. J. Carlin and P. P. Civalleri, *Wideband Circuit Design*. Boca Raton, FL, USA: CRC Press, 1998.

[28] H. Baher, *Synthesis of Electrical Networks*. New York, NY, USA: Wiley, 1984.

[29] I. Hunter, *Theory and Design of Microwave Filters*. London, U.K.: IEE Press, 2001.

[30] R. Levy and I. Whiteley, "Synthesis of distributed elliptic-function filters from lumped-constant prototypes," *IEEE Trans. Microw. Theory Techn.*, vol. MTT-14, no. 11, pp. 506–517, Nov. 1966.

[31] H. Ozaki and J. Ishii, "Synthesis of a class of strip-line filters," *IRE Trans. Circuit Theory*, vol. 5, no. 2, pp. 104–109, Jun. 1958.

[32] R. J. Wenzel, "Exact design of TEM microwave networks using quarter-wave lines," *IEEE Trans. Microw. Theory Techn.*, vol. MTT-12, no. 1, pp. 94–111, Jan. 1964.

[33] M. C. Horton and R. J. Wenzel, "General theory and design of optimum quarter-wave TEM filters," *IEEE Trans. Microw. Theory Techn.*, vol. MTT-13, no. 3, pp. 316–327, May 1965.

[34] B. J. Minnis, *Designing Microwave Circuits by Exact Synthesis*. Norwood, MA, USA: Artech House, 1996.

[35] R. J. Cameron, C. M. Kudsia, and R. R. Mansour, *Microwave Filters for Communication Systems: Fundamentals, Design, and Applications*. Hoboken, NJ, USA: Wiley, 2007.

[36] R. Levy, "Tables of element values for the distributed low-pass prototype filter," *IEEE Trans. Microw. Theory Techn.*, vol. MTT-13, no. 5, pp. 514–536, Sep. 1965.

[37] A. Papoulis, *The Fourier Integral and its Applications (Electronic Science Series)*. New York, NY, USA: McGraw-Hill, 1962.

[38] A. V. Oppenheim and R. W. Schafer, *Discrete-Time Signal Processing*, 3rd ed. New York, NY, USA: Pearson, 2013.

[39] A. V. Oppenheim, A. S. Willsky, and S. H. Nawab, *Signals & Systems*, 2nd ed. Upper Saddle River, NJ, USA: Prentice-Hall, 1997.

[40] D. M. Pozar, *Microwave Engineering*, 3rd ed. New York, NY, USA: Wiley, 2005.

[41] I. Arnedo, M. A. G. Laso, F. Falcone, D. Benito, and T. Lopetegi, "A series solution for the single-mode synthesis problem based on the coupled-mode theory," *IEEE Trans. Microw. Theory Techn.*, vol. 56, no. 2, pp. 457–466, Feb. 2008.

[42] I. Arnedo, I. Arregui, A. Lujambio, M. Chudzik, M. A. G. Laso, and T. Lopetegi, "Synthesis of microwave filters by inverse scattering using a closed-form expression valid for rational frequency responses," *IEEE Trans. Microw. Theory Techn.*, vol. 60, no. 5, pp. 1244–1257, May 2012.

[43] I. Arnedo et al., "Synthesis of one dimensional electromagnetic bandgap structures with fully controlled parameters," *IEEE Trans. Microw. Theory Techn.*, vol. 65, no. 9, pp. 3123–3134, Sep. 2017.

[44] A. Rosenthal and M. Horowitz, "Inverse scattering algorithm for reconstructing strongly reflecting fiber Bragg gratings," *IEEE J. Quantum Electron.*, vol. 39, no. 8, pp. 1018–1026, Aug. 2003.

[45] B. Z. Katsenelenbaum, L. Mercader, M. Pereyaslavets, M. Sorolla, and M. Thumm, *Theory Nonuniform Waveguides—The Cross-Section Method*. London, U.K.: IEE Electromagnetic Waves Series, 44, 1998.

[46] G. H. Song and S. Y. Shin, "Design of corrugated waveguide filters by the Gel'fand-Levitan-Marchenko inverse-scattering method," *J. Opt. Soc. Amer. A, Opt. Image Sci.*, vol. 2, no. 11, pp. 1905–1915, Nov. 1985.

[47] E. Peral, J. Capmany, and J. Marti, "Iterative solution to the Gel'Fand-Levitan-Marchenko coupled equations and application to synthesis of fiber gratings," *IEEE J. Quantum Electron.*, vol. 32, no. 12, pp. 2078–2084, Dec. 996.

[48] J. M. Percaz et al., "General synthesis of tapered matching sections for single-mode operation using the coupled-mode theory," *IEEE Trans. Microw. Theory Techn.*, vol. 67, no. 9, pp. 3511–3526, Sep. 2019.

[49] I. Arregui et al., "High-power low-pass harmonic filters with higher-order TE_{n0} and non-TE_{n0} mode suppression: Design method and multipactor characterization," *IEEE Trans. Microw. Theory Techn.*, vol. 61, no. 12, pp. 4376–4386, Dec. 2013.

[50] M. Salek et al., "W-band waveguide bandpass filters fabricated by micro laser sintering," *IEEE Trans. Circuits Syst. II, Exp. Briefs*, vol. 66, no. 1, pp. 61–65, Jan. 2019.

Jon M. Percaz (Member, IEEE) was born in Pamplona, Spain, in 1985. He received the Telecommunication Engineering, M.Sc., and Ph.D. degrees from the Electrical, Electronic and Communications Engineering Department, Public University of Navarre (UPNA), Pamplona, in 2010, 2015, and 2020, respectively.

His current research interests include coupled-mode theory and inverse-scattering techniques applied to the synthesis of passive devices and structures employed in microwave, millimeter-wave, and terahertz (THz)-wave technologies.

Dr. Percaz received the Pre-Doctoral Grant from UPNA to support his doctoral thesis.

Jabir Hussain was born in Assam, India. He received the bachelor's degree in electronics and telecommunication engineering from Assam Engineering College, Guwahati, India, in 2013, and the master's degree in RF and microwave engineering from IIT Kharagpur, Kharagpur, India, in 2016. He is currently pursuing the Ph.D. degree at the Electrical, Electronic and Communications Engineering Department, Public University of Navarre, Pamplona, Spain, as part of the TESLA Project H2020-MSCA-ITN.

Since 2016, he has worked as a Faculty Member with the School of Electronics Engineering, Kalinga Institute of Industrial Technology, Bhubaneswar, India, where his research included the design and analysis of ultra-wideband filters. His current research interests include the design and synthesis of passive devices for satellite applications, high-power analysis, and additive manufacturing.

Ivan Arregui (Member, IEEE) received the Telecommunication Engineering, M.Sc., and Ph.D. degrees from the Public University of Navarre (UPNA), Pamplona, Spain, in 2005, 2008, and 2013, respectively.

He is currently an Assistant Professor with the Electrical, Electronic and Communications Engineering Department, UPNA. He is the Co-Founder of TAFCO Metawireless S.L., a spin-off company of UPNA. His current research interests include periodic structure devices for microwave, millimeter-wave, and terahertz frequency ranges, numerical techniques for the inverse-scattering synthesis, and the design of passive components for communications satellites.

Dr. Arregui received a grant from the Spanish Ministry of Science and Innovation and several prizes, including the Junior Research Award of UPNA, the HISDESAT Prize from the Spanish Telecommunications Engineers Association (COIT/AEIT) for the Best Doctoral Dissertation in satellite services, and the Innovation Award from the Alberto Elzaburu Foundation.

Fernando Teberio (Member, IEEE) received the Telecommunication Engineering, M.Sc., and Ph.D. degrees from the Public University of Navarre (UPNA), Pamplona, Spain, in 2009, 2011, and 2018, respectively.

From 2009 to 2018, he was with the Electrical, Electronic and Communications Engineering Department, UPNA. He collaborated in several research projects supported by the Spanish Government, the European Space Agency (ESA), and private companies. Since September 2018, he has been with the Alter Technology Group, Sevilla, Spain, and since September 2019, he has been the CTO of the Antennas and Passives Department, Anteral, Pamplona. His current research interests include periodic structure devices and the design and test of passive and active components for communication satellites for microwave and millimeter-wave frequency ranges.

Dr. Teberio received the Network Partnering Initiative (NPI) Grant from the ESA to support his doctoral research and the HISDESAT Prize from the Spanish Telecommunications Engineers Association (COIT/AEIT) for the Best Doctoral Dissertation in satellite communications.

David Benito was born in Huesca, Spain, in 1965. He received the M.Sc. and Ph.D. degrees in electrical engineering from the Polytechnic University of Madrid, Madrid, Spain, in 1992 and 1999, respectively.

Since 1992, he has been an Associate Professor with the Electrical Engineering Department, Public University of Navarre, Pamplona, Spain, where he has been a Full Professor, since 2010. He has coordinated several research projects supported by the Spanish Government and European Union concerning fiber-optic communications and microwave engineering. He has authored or coauthored over 80 international articles and conference contributions. His current research interests include the analysis/synthesis techniques of photonic/electromagnetic-bandgap structures, and their applications to microwave filters and optical communication systems.

Petronilo Martin-Iglesias (Senior Member, IEEE) was born in Cáceres, Spain, in 1980. He received the Telecommunication Engineering degree from the Polytechnic University of Madrid, Madrid, Spain, in 2002, and the master's degree from the University of Leeds, Leeds, U.K., in 2012.

He has been working in industry for over ten years as a Microwave Engineer involved in active (high-power amplifiers for radar applications) and passive (filters, multiplexers, and couplers) RF hardware design, including two years as a Radar System Engineer with Indra Sistemas, Madrid, ISDEFE S.A., Madrid, and Thales Alenia Space Spain, Madrid. Since 2012, he has been with the European Space Agency, Noordwijk, The Netherlands, where he is involved in the research and development and project support activities related to RF passive hardware developments. His current research interests include filter synthesis theory, electromagnetic (EM) design, high-power prediction, as well as advanced manufacturing techniques for RF passive hardware.

Mr. Martin-Iglesias has been serving as a member of the IEEE Microwave Theory and Techniques Society (IEEE MTT-S) Technical Program Committee (TPC) since 2013.

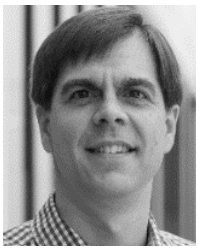

Israel Arnedo (Senior Member, IEEE) was born in Tudela, Spain, in 1980. He received the Telecommunication Engineering, M.Sc., and Ph.D. degrees from the Public University of Navarre (UPNA), Pamplona, Spain, in 2004, 2007, and 2010, respectively.

He is currently an Associate Professor with the Electrical, Electronic and Communications Engineering Department, UPNA, where he has managed and participated in research projects supported by the Spanish Government, the Natural Sciences and Engineering Research Council of Canada (NSERC), the European Commission, and private companies. Since 2018, he has been the Vice-Dean of the School of Engineering, UPNA. He is the Co-Founder of TAFCO Metawireless S.L., a spin-off company of UPNA. He holds two international patents successfully licensed. He has authored or coauthored more than 75 articles. His current research interests include microwave, millimeter-wave, and terahertz fields that include periodic structure devices, coupled-mode theory, inverse-scattering synthesis, material characterization, and their applications in ultra-wideband (UWB) systems, space and satellite technology, biomedical engineering research, and industrial products.

Dr. Arnedo was a recipient of the Formación de Profesorado Universitario (FPU) Grant of the Spanish Ministry of Education and Science to support his doctoral research, the José Castillejo Grant of the Spanish Ministry of Education to support his post-doctoral research stay at the Institut d'Électronique de Microélectronique et de Nanotechnologie (IEMN), Villeneuve-d'Ascq, France, in 2012, and the Junior Research Award of UPNA for the Best Doctoral Dissertation in engineering in 2014. He is a reviewer for several international scientific journals.

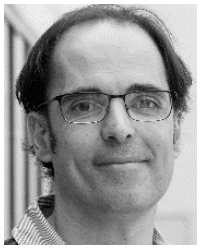

Miguel A. G. Laso (Senior Member, IEEE) received the M.Sc. and Ph.D. degrees in telecommunications engineering from the Public University of Navarre (UPNA), Pamplona, Spain, in 1997 and 2002, respectively.

From 1998 to 2001, he was a Doctoral Fellow Student with the Electrical and Electronic Engineering Department, UPNA, where he was an Assistant Professor from 2001 to 2006 and has been an Associate Professor (Professor Titular) since 2006, always involved in teaching and research duties related to optical communications and microwave engineering. From 2002 to 2003, he was also a Research Fellow with the Payload Systems Division, European Space Research and Technology Centre, European Space Agency (ESTEC-ESA), Noordwijk, The Netherlands. He is currently the Head of the Microwave Components Group (MCG), UPNA. He is the Co-Founder of TAFCO Metawireless S.L., a spin-off company of UPNA. He has authored or coauthored dozens of journal articles and contributed to major international conferences. He has also led projects with public and private funding within the MCG and UPNA. He holds several international patents. His current research interests include periodic structures, inverse scattering problems, synthesis techniques for filters and multiplexers in the microwave and millimeter-wave frequency ranges, and their applications in wireless and space communications.

Dr. Laso has received several prizes, including the Spanish National Prize to the Best Doctoral Dissertation in telecommunications from the Spanish Telecommunications Engineers Association (COIT/AEIT) in 2002, the Junior Research Award of UPNA in 2003, and the 2005 Spanish National Prize for the Best Project in Innovation in Higher Education from the Spanish Ministry of Education and Science. He was an Associate Editor of IEEE TRANSACTIONS ON MICROWAVE THEORY AND TECHNIQUES from 2019 and 2022, and he is the current President of the URSI Spanish National Committee. He is also a member of several professional and scientific international associations, including the Optical Society of America (OSA), the International Society for Optics and Photonics (SPIE), and the American Society for Engineering Education (ASEE). He is also a TPRC Member of the MTT-S International Microwave Symposium (IMS) and a reviewer for several other international conferences and journals. He was the Co-Chair of the EuMC'18 (Madrid) and the Education Resources Development Subcommittee and is a member of MTT-5 Filters and the MTT-S Education Committee. He is also the Chair of the Working Group of Standards for Microwave Filter Definitions, IEEE Standards Committee.

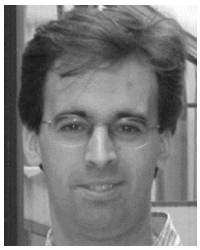

Txema Lopetegi (Member, IEEE) was born in Pamplona, Navarre, Spain, in 1973. He received the M.Sc. and Ph.D. degrees in telecommunication engineering from the Public University of Navarre (UPNA), Pamplona, in 1997 and 2002, respectively.

Since 1997, he has been an Assistant Professor with the Electrical, Electronic and Communications Engineering Department, UPNA, where he has been an Associate Professor since 2006. From 2002 to 2003, he was a Research Fellow with the Payload Systems Division, European Space Research and Technology Centre (ESTEC), European Space Agency (ESA), Noordwijk, The Netherlands. He is the Co-Founder of TAFCO Metawireless S.L., a spin-off company of UPNA. His current research interests include metamaterials and synthesized structures in microwave, millimeter-wave, and terahertz (THz) technologies, filters and passive components, coupled-mode theory and synthesis techniques using inverse scattering, and their applications in wireless and space communications.

Dr. Lopetegi received a grant from the Spanish Ministry of Education in 1999 and 2000 to support the research in his doctoral thesis, several prizes including the Spanish National Prize to the Best Doctoral Dissertations in telecommunications in 2003 awarded by COIT/AEIT, and the Extraordinary Doctorate Prize of UPNA.